LUND UNIVERSITY

LTH

FACULTY OF ENGINEERING

Lund University
Faculty of Engineering
Department of Physics
Division for Atomic Physics
Thesis submitted for the degree of Master of Science
Engineering Physics
LRAP 569

Black phosphorous sample preparation for ultrafast electron diffraction studies

by
Rebecca Ahrling

Supervisor: *Jörgen Larsson*
Assistant supervisor: *Åsa Bengtsson*
Examiner: *Cord Arnold*

August 2020

Acknowledgements

I would like to thank my supervisor professor Jörgen Larsson for his great insight and ideas, and for seeing the small details. A special thank you to my assistant supervisor Åsa Bengtsson, for all the support and always being available for support and discussions. And to Eric Nilsson and Carl Ekström, thank you for answering questions and I wish all of you good luck with future projects and I am looking forward to seeing the results. I would also like to extend my thanks and appreciation to the entire division of atomic Physics, even during these extraordinary times and especially to Åke Johansson for the support.

Finally, I want to thank my family and friends, who have always supported and believed in me, even if what I have done haven't always made sense to you.

Abstract

Since 2004 when mechanical exfoliation was first utilised to produce single layered samples of graphite, 2D materials have gained interest in the scientific community. With the prerequisite that the initial bulk material has a layered structure, these 2D materials have created an opportunity to examine materials on a very small scale as well as opening the possibility of creating smaller electrical components for industrial and commercial use, with well-known and documented parameters. Graphene is known to be strong and is used for batteries, while black phosphorus has potential as a semiconductor, due to the variable band gap, which is dependent on the number of layers of the material, as well as good mobility. In this project, the goal is to identify a method for mechanically exfoliating samples of graphite and black phosphorus and suspending these, by transferring the samples to a copper grid. These suspended samples are prepared for the purpose of experiments using ultrafast electron diffraction. This type of experiment is used to understand heating of a material for optronics applications.

Popular science summary

In 2004, scientists found a way to easily create very thin samples of certain materials, which is called mechanical exfoliation. The first one was thin layers of graphite, and the method was to simply use two pieces of tape to peel down the graphite until only a single layer of atoms remained on the tape. Single layered graphite now has a special name: graphene. Graphene is not the only material that can be peeled down using this method, and all these materials together are now called 2D materials.

2D materials are of interest since they make it possible to create very small electrical components. 2D stands for two dimensional, and means that the material can cover a surface, but is so thin that in some cases the layer only consists of a single atom. In the industry this is of great use, since smaller components mean that computers e.g. can be made smaller. 2D materials are also be used to create better batteries, which is especially important for the automotive industry when electrical vehicles are becoming more popular.

Graphene is the first material in this category, which means that it is also the most well-known and well-studied material. But other materials have similar properties, and different materials are more suitable for different purposes.

One new material, which was rediscovered in 2014, is black phosphorus. Black phosphorus is a very interesting material, since it is possible to change the so-called band gap by changing how thick the material is. The band gap means how much energy you have to apply for electricity to run through the material. This is something that cannot be done with graphene, so black phosphorus has the potential to be even better for electrical components than graphene. Another interesting thing about black phosphorus is that 1 % of the human body is composed of phosphorus. Black phosphorus therefore has the potential to be used as a biodegradable material in the human body, for bio-imaging or photodynamic therapy. Potentially, this could be used to locate cancer cells without introducing any new harmful chemicals. The biomarker would then be broken down in the body naturally over time. But in order for black phosphorus to replace graphene or be used in biomedical science, more research has to be performed.

One way to examine black phosphorus is to first use mechanical exfoliation to create very small flakes, and then placing these flakes on grids. If this is done, it is possible to mount the flake, so that it almost seems like it is suspended freely in the air. This means that no other material is in the way to disturb the measurement.

There are different ways to examine a material. One way is to use a laser to shoot at the flake, and for example look at how much weaker the laser is after than before, or how different it is if you change the direction the laser hits the flake. Another way is to use electrons. By using a so called electron gun, a bunch of electrons can be directed to the flake, and then it is possible to look at how they have changed direction after hitting the flake. Since the flakes are very thin, almost every electron can pass through the material, but not every electron can pass without hitting at least one atom. And by finding how much the electrons have been deflected from the initial path, it can actually be calculated how close the atoms are to each other in the flake.

Contents

Acronyms

BP - Black phosphorus

PMMA - Poly(methyl methacrylate)

IMFP - Inelastic mean free path

2D - Two dimensional

AC - Armchair

ZZ - Zigzag

1 Introduction

With 2D layered materials gaining interest and finding applications in the industry, it is of importance to understand the structure and finding the relevant properties of these materials, in order to optimise usage in different applications. Thus, it is valuable to prepare samples with the purpose of finding these parameters.

This project describes a reliable method for suspending flakes of 2D layers materials, and finding the critical points of the process in order to suspend as optimal flakes as possible. In short, the process consists of acquiring small flakes of the material, which requires a material that has a layered atomic structure. These flakes has to be transferred onto the desired substrate, which in the case of this project is a copper grid. Methods for performing the necessary measurements in order to find thickness and orientation of the suspended flake in order to be able to interpret signals from later measurements were also investigated. Since the flakes used in this project are suspended onto a small copper grid used for electron diffraction, the thickness is compared to the penetration depth of electrons in a material.

Electron diffraction is a type of experiment where a beam of electrons are directed at a sample. As they pass through a material, there is a probability of the electrons being scattered, or diffracted. From elastic scattering, the angle of the scattered electrons give information about the distance between atoms in the unit cell of the crystalline structure. By observing inelastic scattering, the orientation of a sample can be specified. For this project, the electrons are assumed to have an incident energy of 58 keV, as this is the energy of the set up for which the samples are prepared, and samples are prepared to measure the distance between atoms in the unit cell. This means that limits has to be placed on the sample preparation when it comes to thickness, in order to allow electrons to pass through and scatter elastically, but not inelastically. The lateral area of the samples are of interest as well. The size of the assumed electron beam is 200 µm in diameter. While the sample does not need to be this big, as there is still going to be diffraction seen from a smaller sample, a larger sample is useful in order to better find a spatial overlap between sample an incident electron beam.

1.1 2D materials

2D materials surged in interest in the scientific community in 2004 when Novoselov et. al. [1] showed a straight forward way of performing mechanical exfoliation to reliably produce few layered flakes of graphite. The simple method presented by Novoselov et. al. [1] opened up easy access to perform experiments on this type of material. In short, the method consists of placing a small bulk of the material in question onto a piece of tape, and by folding the tape over the material and pulling them apart and repeating this process creating thinner and thinner flakes until they can be counted as single or few layered. This method has been shown to be applicable for other materials which show the same 2D layered structure, amongst others boron nitrade (BN) and molybdenum disulfide (MoS_2). [2] This method works by the layers having strong intralayer bonds, usually ionic, and weaker interlayer bonds such as van der Waals forces. [3] This creates a material that is sensitive to shear force, as seen in figure 1, which shows the principle of how to separate the layers of a layered structure. Experiments performed on 2D layered materials provide valuable knowledge of parameters such as band gap, carrier mobility and on-off carrier ratio, and 2D materials are also of interest in the electronics industry, where graphite has been previously used [2].

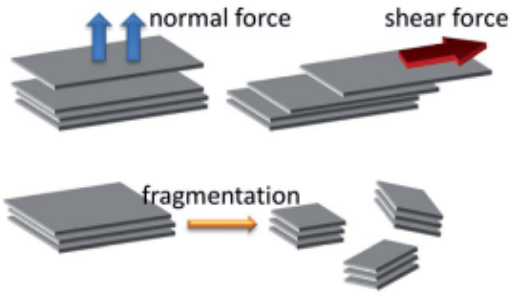

Figure 1: The layered structure of a 2D material, and a visual representation of how the layers can be separated. Image reproduced from reference. [4]

1.1.1 Graphite

Single layered graphite are in most instances referred to as "graphene". [5] Presently, graphene is arguably the most common and well-known 2D material. Graphene is a so-called allotrope of carbon. An allotrope is a structural variation of the same atoms, meaning that one element can have different forms while still being in the same state depending on the bonds. Carbon is a good example of this, with diamond, graphite and fullerenes being some of the most well-known allotropes. Of the allotropes of carbon, graphite is the only to exhibit the layered tendency. The structure of hexagonal graphite can be seen in figure 2, where the structure of the layers can be seen. While graphene has been shown to have many usages [2], one of the main drawbacks is the lack of a band gap. A band gap is the threshold beneath which no current can run through a material. In short, this means that graphene is always conductive, leading to a lack of no on-off current ratio. This hampers the use of graphene as a material for transistors. These parameters are shown together with parameters for black phosphorus and silicon in table 1.

1.1.2 Black phosphorus

Black phosphorus (BP) has gained interest since 2014 [7] [8] [9] [10], and is one of the three main allotropes of phosphorus: white, red and black phosphorus. Of the three, black phosphorus is known to be the most thermodynamically stable. [3] For the purpose of applications, one of the most interesting parameters of BP is the variable band gap. The band gap of BP varies from around 0.3 eV for bulk, up to 2.15 eV for single layered BP, also referred to as phosphorene. [11] This makes BP an interesting component in electronics, as this would provide better control of the behaviour of smaller structures. This band gap is due to the structure of the layers, as can be seen in figure 3, which compared to the flat layers of graphite can be described as puckered. [7]

However, despite the recent interest in BP, there are still several unknown parameters of BP, such as the heat dissipation behaviour on an ultrafast scale. One of the main problems facing BP as a competitor to other 2D material is the degradation process during ambient conditions. Ambient conditions here is used to refer to room temperature, atmospheric pressure and normal levels of humidity. [13] [11] [7] The degradation is caused by sublimation and not melting and BP samples of around 10 nm thickness show signs of degradation within a few days, and thinner samples showed degradation within hours in ambient conditions. [3] [14] During the degradation process, small droplets appear on the surface of the BP sample [13], and these first signs of degradation could be removed by storing the samples in vacuum [11], however, instability such as this limits the use in consumer products, since currently the only way to avoid degradation is storing the samples in vacuum and not exposed to light. One interesting application of BP is as a field effect

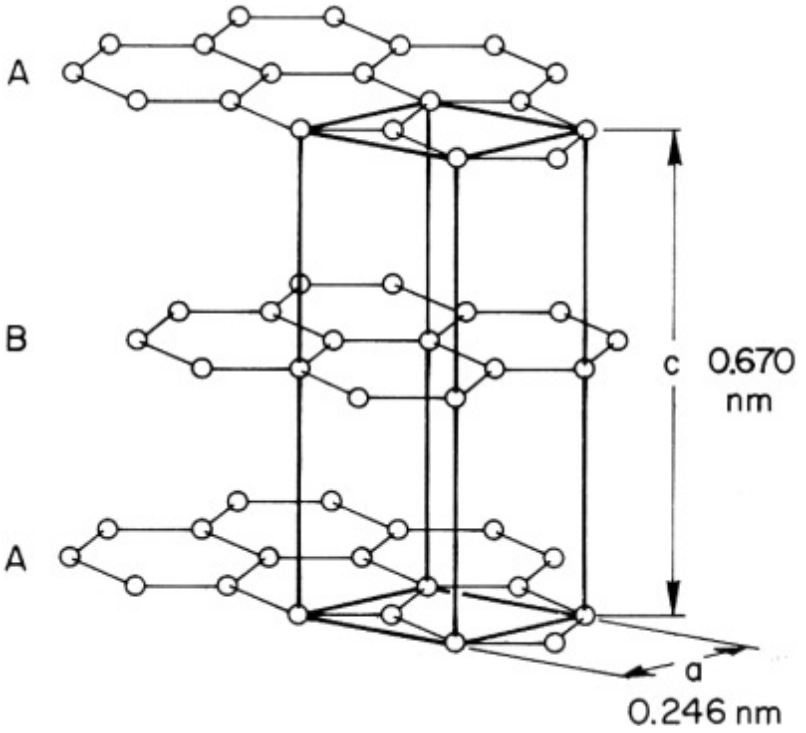

Figure 2: The structure of the layers of graphite. The atoms are bound in a hexagonal pattern. Image reproduced from reference. [6]

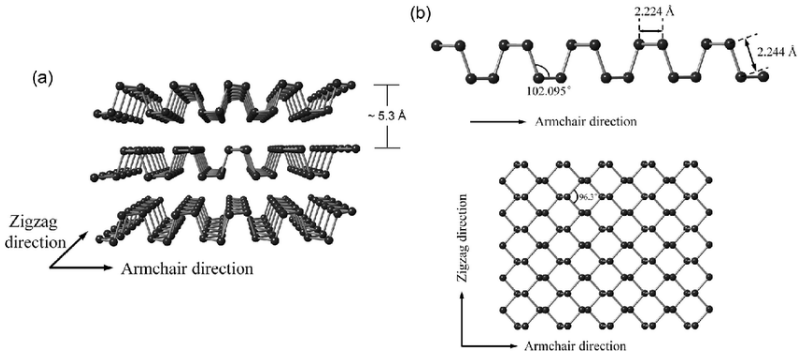

Figure 3: The layered structure of black phosphorus. To the left the armchair structure can be seen and to the lower right the top down view more easily show the zig-zag direction. Image reproduced from reference. [12]

transistor [15], as BP has been described as a potential replacement of silicon [8], and within the biomedical field, as phosphorus is naturally occurring in the human body, this could potentially lead to naturally degrading biomarkers and biosensors [16].

	Black phosphorus	Graphene	Silicon
Bandgap (eV)	0.3-2	0	1.11
Carrier mobility ($cm^2V^{-1}s^{-1}$)	1000	0	
On/off current ratio	10^3-10^5	200 000	$4{\cdot}10^4$
Thermal conductance ($Wm^{-1}K^{-1}$)	36 (110)	2000/5000	149

Table 1: Comparison of some parameters of black phosphorus, graphene and silicon. [8]

2 Theory

2.1 Thickness of sample

To be able to acquire results from experiments with a sample, the sample should be suspended in free air to minimise interactions with other materials which could otherwise affect the results, and the thickness has to be within the range of thick enough to allow interactions to happen and thin enough to be able to allow either photons or electrons through, depending on the type of experiments performed and the criteria is dependent on this. As the samples are prepared for use in electron diffraction, where electrons are accelerated and focused onto the sample, the target thickness is estimated with this in mind. Due to the fact that electrons are light particles, the momentum transfer is small, however the energy loss is large, which means that the penetration depth of electrons in a material can be derived from the energy loss equation. [17]

There are two main interactions to take into account: elastic and inelastic scattering. Elastic scattering causes no loss from the incident energy, and this type of scattering causes the diffraction pattern seen in figure 4. The incident energy of the electrons that produced the figure was 58 keV. As this incident energy is used in the lab the samples for this project are prepared for, this was chosen as the point of reference for the limits for the thickness.

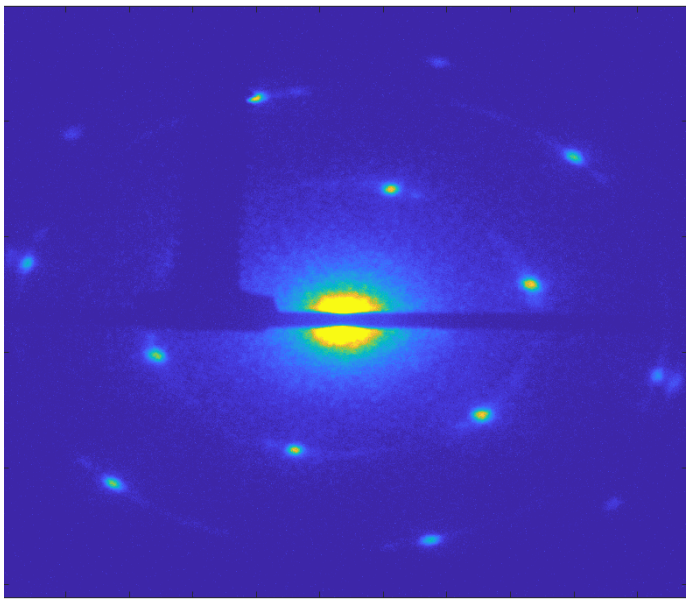

Figure 4: Diffraction pattern of graphite for electrons of incident energy 58 keV.

The diffraction pattern shows how much the electrons are deflected and by using Bragg's law $2d\sin\Theta = n\lambda$ for the angle of scattering Θ, the wavelength of the electrons λ and the number of layers n, the spacing between layers d can be calculated, which is the distance between planes

for the unit cell. Therefore, the main goal for observing the electron diffraction pattern is finding the distances within the unit cell of a crystalline structure.[18] By calculating how long it takes for an elastically scattered electron to dissipate in a material, the allowed thickness of a sample can be estimated. However, the inelastically scattered electrons can give rise to so-called Kikuchi lines. To know the possible impact of these lines, the probability of elastic and inelastic scattering must be known, however, this information was not found for the case of scattering of electrons. By examining the range of elastically and inelastically scattered electrons, some assumptions of the possible thickness of a material can be made. Kanaya and Okayama expresses the range R for elastic scattering as

$$R = \frac{\rho \cdot 5.025 \cdot 10^{-12} A E_0^{5/3}}{\lambda_s Z^{8/9}} \cdot \frac{(1 + 0.978 \cdot 10^{-6} E_0)^{5/3}}{(1 + 1.957 \cdot^{-6} E_0)^{4/3}} \tag{1}$$

where ρ is the density of the material, R is the range in meters, E_0 as the incident energy of the electrons, A the atomic weight and the atomic number$Z$. The value of λ_s was chosen as 0.182, as this gave a good generalisation that agreed with experiments, according to Kanaya and Okayama. [17] E_0 is the incident electron energy. The second term gives the relativistic corrections of the formula. [17] The results from this formula gives the total distance an electron can pass through a certain material, with the possibility of an electron going almost straight through. This means that a sample of this thickness would let some single electrons through, while a thicker sample would deny any electrons from passing. In figure 5, the maximum penetration depth is plotted as a function of the incident electron energy in keV. A few different materials have been plotted for comparison, and it can be seen that the heavy materials such as iron, gold and copper have a lower maximum range than the lighter materials aluminium, carbon and black phosphorus. For 60 keV, the value chosen to be a reference point for this project, the maximum range of BP can be read as around 30 µm. If the assumption is made that the incident electron only scatter elastically, this would be the maximum range allowed for the material.

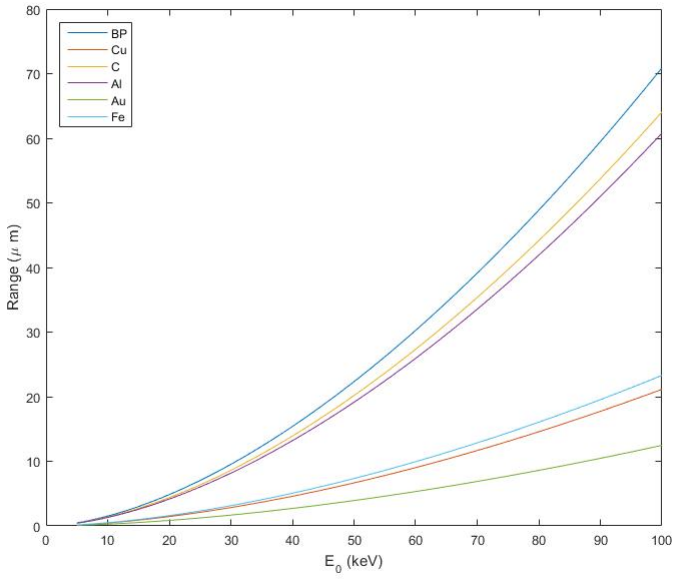

Figure 5: The maximum range for different materials in µm as a function of incident electron energy keV

However, as the maximum range is indeed the maximum range, the probability of an electron

penetrating this deep is low. To better describe the more likely depth, the loss of energy of an electron can be examined. The energy of the electrons at a given depth can be expressed by the following equation, which describes the loss of energy of an electron for the reduced depth $y = x/R$

$$E = (1 - y)^{3/5} E_0 \tag{2}$$

From the loss of energy, the diffusion depth x_D, which denotes the depth in a material where the transmitted fraction is equal to 1/e, can be given by

$$x_D = \frac{R}{1 + \gamma} \tag{3}$$

for $\gamma = 0.187 Z^{2/3}$. [17] The diffusion depth x_D as a function of the incident electron energy can be seen in figure 6. Compared to the maximum range of 30 µm for BP, the diffusion depth is 15 µm. As the maximum range gives the highest possible distance travelled in a material, diffusion depth is more in line with the possibility of enough electrons for a measurement to contain information.

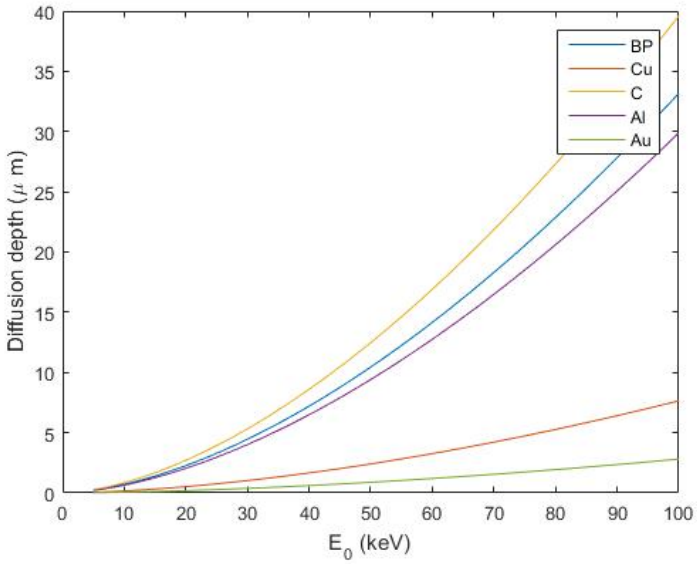

Figure 6: The diffusion depth as a function of incident electron energy in keV for different materials.

The inelastic mean free path describes the distance an electron can travel before losing all of the incident energy. Inelastically scattered electrons as compared to elastically scattered electrons loses energy compared to the incident electron energy, and have the potential to give rise to Kikuchi lines. When an electron is scattered inelastically with a small angle, and then again scattered elastically, this creates Kikuchi lines. [18] While Kikuchi lines can be used to identify the orientation of a sample, these lines causes problems if the purpose is to identify the spacing between layers in a material. [18] [19] Tanuma et. al. gives the following formula for the IMFP λ in Ångström

$$\lambda = \frac{E}{E^2[\beta \ln(\gamma E) - \frac{C}{E} + \frac{D}{E^2}]} \tag{4}$$

where E is the electron energy in eV, E_p is the bulk plasmon energy in eV, and β, γ, C and D are material specific parameters given as follows by Tanuma et. al.

$$\begin{aligned}
\beta &= -0.10 + \frac{0.944}{(E_p^2 + E_g^2)^{0.5}} + 0.069\rho^{0.1} \\
\gamma &= 0.191\rho^{-0.5} \\
U &= \frac{E_p^2}{829.4} \\
C &= 1.97 - 0.91U \\
D &= 53.4 - 20.8U
\end{aligned} \tag{5}$$

where E_g is the band gap in eV. The equations for β, γ, U, C and D were acquired experimentally by Tanuma et. al., equation 4. The IMFP of graphite, white phosphorus and black phosphorus can be seen in figure 7, and for BP the IMFP is 76 nm. A summary of the maximum range, the diffusion depth and the IMFP for graphite and BP for incident electron energy 60 keV can be seen in table 2. As can be seen in the table, an elastically scattered electron have a longer reach than an inelastically scattered electron. The probability for the different types of scattering depends on the structure of the material, however as a thicker sample naturally gives a higher probability of interactions, the thicker the sample is, the higher the probability of unwanted Kikuchi lines [18]. As the Kikuchi lines appear by first inelastic scattering followed by elastic, this means that having a sample that is thinner than the IMFP reduces the likelihood of Kikuchi lines appearing in the measurement, in the case of BP this means that the goal is to have a sample thinner than 76 nm. Conversely, if the purpose of the measurement is to find the Kikuchi lines, the sample should be more than the IMFP to allow inelastic interactions to occur.

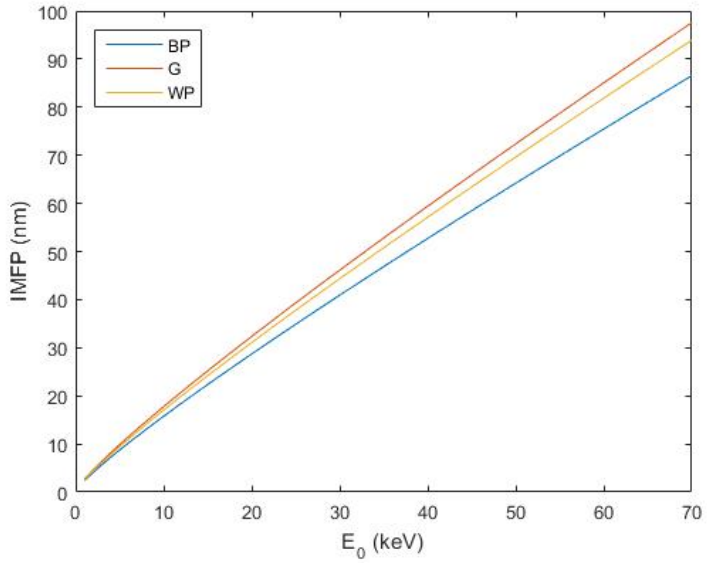

Figure 7: The inelastic mean free path of white and black phosphorus as well as graphite as a function of incident electron energy in keV.

To calculate the thickness of a sample which has already be suspended, it is possible to use Beer-Lambert's law as follows

	Black phosphorus	Graphite
R	30 µm	27 µm
x_D	14 µm	17 µm
IMFP	76 nm	85 nm

Table 2: The maximum range, the diffusion depth and the IMFP of black phosphorus and graphite for electrons of incident energy 60 keV.

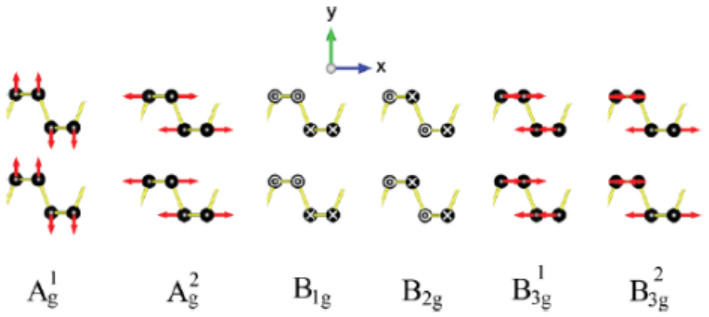

Figure 8: The Raman modes of BP, as seen in the AC direction. Image reproduced from reference. [20]

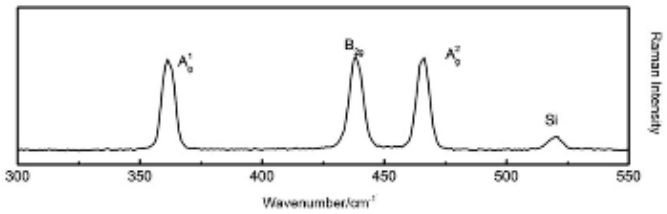

Figure 9: The Raman peaks of the A_g^1, B_{2g} and A_g^2 modes. Image reproduced from reference. [21]

$$I = I_0 \exp(-\alpha \cdot z) \tag{6}$$

For I_0 as the incident intensity and I as the transmitted intensity, α as the absorption coefficient and z as the thickness of the sample. Due to the structure of BP, there is a different absorption coefficient depending on the incoming polarisation of the light. [22] [23] Depending on the polarisation, the intensity of the different Raman modes changes. The Raman modes of BP can be seen in figure 8, and these different modes corresponds to different peaks in a spectrum, as seen in figure 9.

2.2 Orientation measurement with Raman spectroscopy

Raman spectroscopy is a method of finding which kind of atoms are present in a material. This can be done as all atoms are unique, and emit different wavelengths after absorbing light. Thus different emitted wavelengths corresponds to different atoms. While this can be used in order to locate trace components in some cases, for this project the material is known, and the wavelengths of the emitted Raman modes are known. The intensity in this case is therefore used not in order to know whether there is BP in the sample, but rather to examine the intensity of the emission.

By considering the relevant Raman modes of BP, the orientation of the sample can be determined. The intensity of the different Raman peaks are dependent on the incoming polarisation of light as seen in figure 10. To the left the intensity for parallel polarised light is shown and to the right is cross-polarised. Parallel and cross-polarised refers to the angle between the polariser placed before and after reflection of the material the measurement is performed on, where parallel means that they have the same orientation, and cross-polarised refers to the polarisers being rotated perpendicular to each other. If one allow BP to absorb a laser, the BP is going to emit different wavelengths, and these wavelengths are going to correspond to different Raman modes. With the use of a spectrometer, the intensity of the peaks can be recorded. If the polarisation of the incident laser is then changed, it is expected that the intensity should change as seen in the figure.

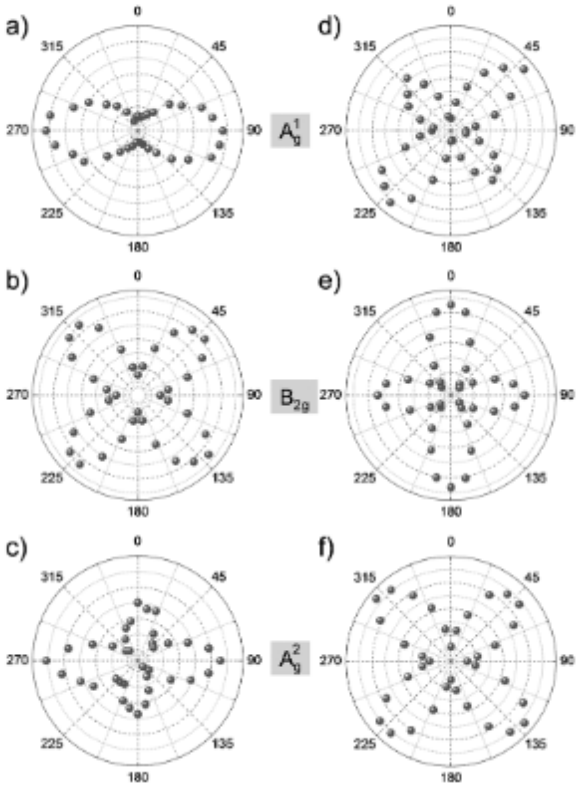

Figure 10: The polarisation dependence of the A_g^1, B_{2g} and A_g^2 modes modes of black phosphorus for parallel and cross-polarised light. Image reproduced from reference. [24]

As seen in the figure, the intensity of the Raman modes are periodic, with different behaviours depending on the mode in question. For the A_g^1 mode, the period is 180 degrees, and for cross-polarised the period is 90 degrees, with two peaks having higher intensity.

3 Method

The focus of the project is how to prepare samples of suspended 2D materials, for the purpose of further experiments. Two types of commercially available forms of BP were examined, using mechanical exfoliation from bulk material of graphite and black phosphorus and a pre-prepared solution of black phosphorus.

3.1 Sample preparation

A step by step process of preparing suspended thin layers of 2D materials was presented by Gonçalves et. al.[25], and provides a baseline of the method used. In short, the method consists of using the so-called mechanical exfoliation method to acquire few-layered flakes of a 2D material, transferring these to a PMMA film, and after locating the flakes, applying a grid and dissolving the PMMA, leaving a small grid with the sample. A summary can be seen in figure 11

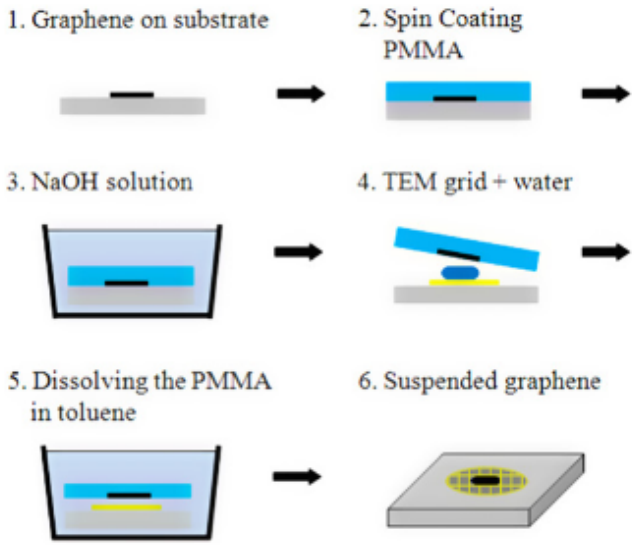

Figure 11: A short presentation of the steps, which provided the outline for the method presented. Image reproduced from reference. [25]

3.1.1 Mechanical exfoliation

The material needed for the mechanical exfoliation is *Micronova™CR100 PC™Cleanroom* Tape, tweezers for handling, a silicon wafer and bulk of the sample material. The bulk material used is graphene and black phosphorus (BP) from *HQ Graphene*. During preparation, every work surface is covered with sheets of aluminium foil, and latex gloves are used for handling. Whenever BP is handled, a face mask is used due to the unknown health effects of inhaled BP. [26] Acetone and isopropanol were used to prepare clean Si wafers, and the chemicals used are kept under a fume hood. [27] [28]

To prepare the sample, the first step is to acquire few layered BP. This is done by mechanical exfoliation, otherwise known as the scotch tape method, the method used by Novoselov et. al. to easily prepare single to few-layered graphite [1]. This is to be done for graphite and BP, and due

Figure 12: The bulk piece of black phosphorus used for exfoliation. When not used, is stored in vacuum in a dark container.

Figure 13: The bulk material as placed on the tape. It is placed and pressed down slightly, and then carefully exfoliated using tweezers.

Figure 14: The tape is pressed together and drawn apart.

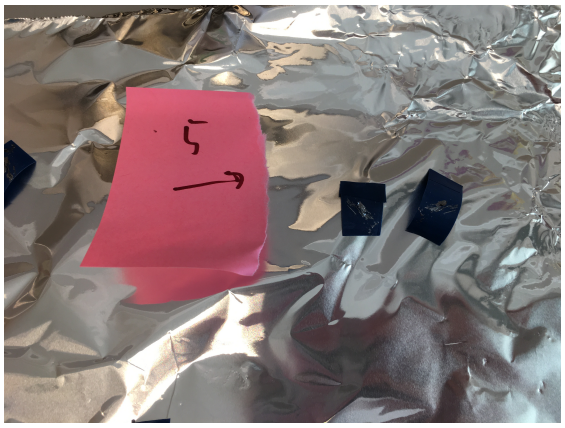

Figure 15: The tape is placed next to the number corresponding to the total exfoliations.

to the similarities in structure, the method remains the same. Mechanical exfoliation refers to the process of placing a piece of the bulk material, such as the one seen in figure 12, and placing it onto a piece of tape, as seen in figure 13. When the bulk material has been removed, the tape now hold a sheet of the material. The tape and material is pressed together and then carefully drawn apart, resulting in figure 14, where it can be seen that the original sheet has been exfoliated into two mirrored pieces. This method of pressing tape together and exfoliating them was repeated to one less than the desired number of exfoliations, as the last exfoliation will be done on the Si wafer. In order to keep track of the number of exfoliations, the majority of the exfoliation was done on smaller pieces of tape, which were cut and then one of the ends were folded over in order to create a small adhesion free handle. Once a piece of tape had been used for exfoliation, it was placed by the corresponding number as seen in figure 15, which shows BP exfoliated a total of 5 times placed on the small pieces of tape.

For the purpose of examining the impact of different number of exfoliations, pieces of tape with 2D materials with 6 and 7 number of exfoliations are prepared for graphite and 6, 7 and 8 are prepared for BP. These small pieces of tape and either graphite or BP is then placed onto an Si wafer. For the etching process, it is important to have a layer of SiO_2 between the wafer and 2D material. [25] This layer is assumed to grow naturally on the wafer. [29] The Si wafers were cleaned before

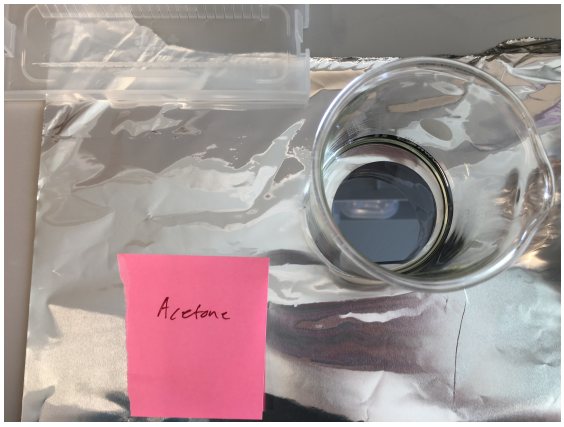

Figure 16: The silicon wafer is cleaned in acetone for 2 minutes.

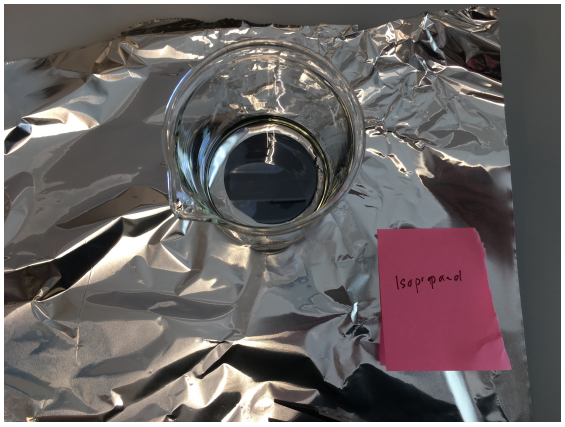

Figure 17: The silicon wafer is rinsed in isopropanol for 20 seconds.

applying the tape. First, they were allowed to soak in acetone for 2 minutes, as seen in figure 16, and afterwards cleaned with isopropanol for 20 seconds, as seen in figure 17. [30] The wafers were allowed to dry before applying the tape. An example of the placement of tape on a silicon wafer can be seen in figure 18.

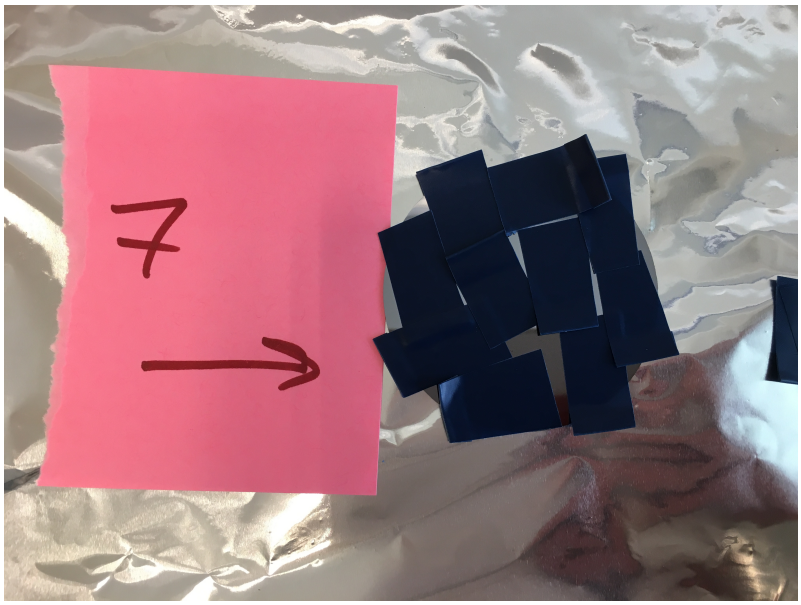

Figure 18: The placement of tape on the silicon wafer. To the left the total number of exfoliations for this particular sample is shown to be 7.

3.1.2 Hotplate

The silicon wafer with the tape is placed on a hotplate turned to 120 degrees C for 2 min, which can be seen in figure 19. This causes the adhesive on the tape to melt. After 2 min, the wafer is removed and allowed to cool to room temperature, after which the tape was removed. With the tape removed as in figure 20, the wafer was once again cleaned, with the purpose of removing as much adhesive residue as possible. The wafer was cleaned in acetone for 20 minutes to dissolve the

tape residue and rinsed in isopropanol for 30 sec, and compared to figure 20, the cleaned wafer in figure 21 shows less signs of tape residue. [30] Once the pieces have been transferred to the silicon wafer, according to Castellanos-Gomez et. al. [11], the flakes are now not at any risk of being rinsed off.

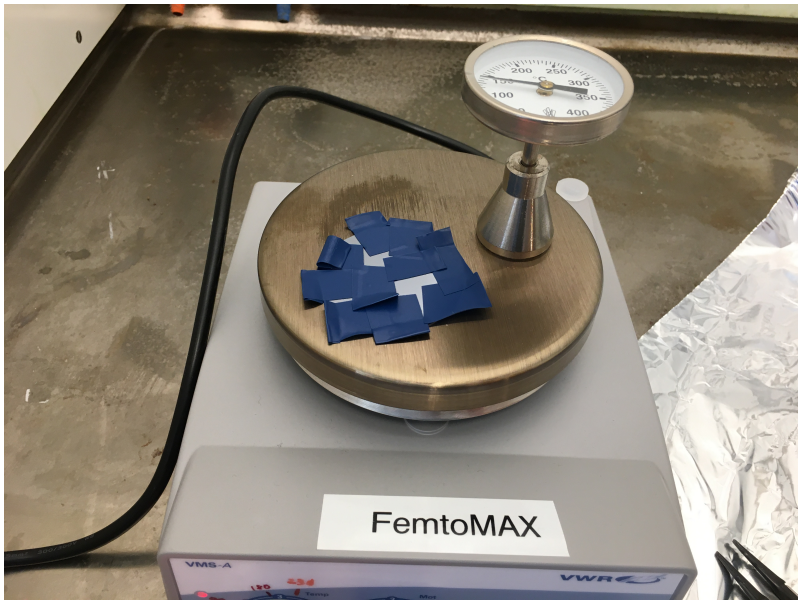

Figure 19: The hotplate used to melt the adhesive of the tape. It is set to 120°C and the wafer is heated for 2 minutes.

To test the importance of this step, a wafer will be prepared that has not been placed on the hotplate. The assumption made is that the 2D material flakes will be bound stronger to the tape due to the adhesive material, which silicon lacks. The melting of tape is assumed to allow the adhesion to become somewhat similar in strength. The step of removing the tape from the wafer is counted as the final exfoliation.

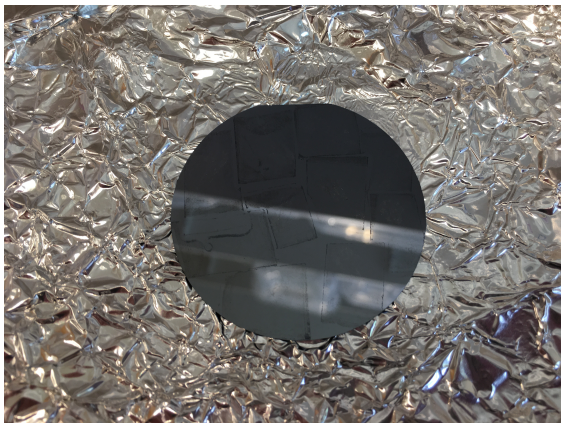

Figure 20: The tape is removed from the wafer, and there remains tape residue across the surface.

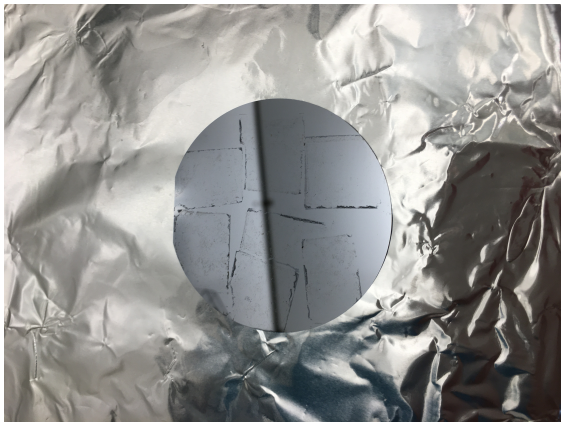

Figure 21: After cleaning, most of the tape residue has been removed, except for the thicker areas that were along the edges of the tape pieces placed on the wafer.

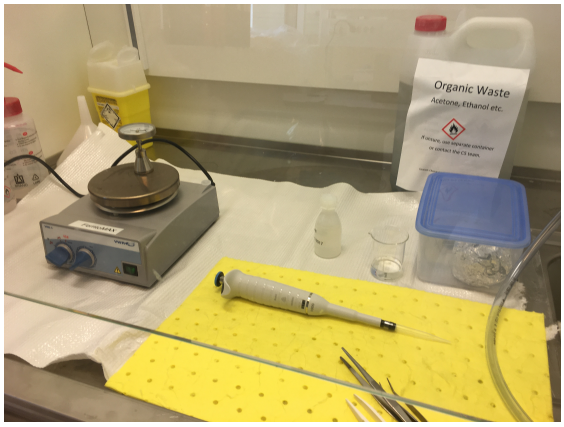

Figure 22: The work space prepared for applying PMMA onto the wafer.

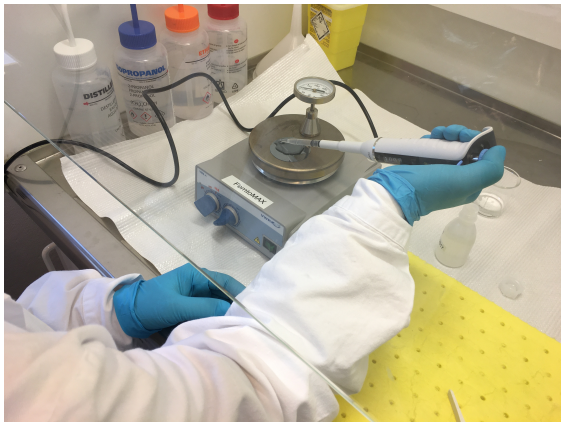

Figure 23: The wafer placed on the hotplate, which allows the liquid PMMA to solidify.

3.1.3 Applying PMMA

Next in the transfer process is moving the flakes from the silicon wafer to a PMMA film. The first step in this process is covering the silicon wafer with PMMA and baking the film by using an oven, to solidify the PMMA. The work space prepared can be seen in figure 22, which shows the hotplate, turned to 120 degrees C, the pipette used to distribute the PMMA liquid. The entire process was kept under a fume hood, due to the danger of inhalation of PMMA fumes and as PMMA is reactive to aluminium, the work surface was also covered with a plastic sheet for this step. [31] Gonçalves et. al.[25] reports using spin coating to cover the silicon wafer with PMMA, however, this was quickly found to provide a too thin layer, which proved to be brittle due to the composition of this particular PMMA. In figure 23, the method of applying the PMMA with a pipette can be seen.

Once the entire wafer is covered in PMMA, it is allowed to solidify on the hotplate, see figure 24, and a total of 4 layers is applied, which gives a thickness of PMMA that allows for the film to be moved without breaking once it has been dried. With use of the hotplate, the PMMA is solidified, however, to ensure that the film is completely solidified throughout, the wafer with the PMMA is placed inside an oven. The oven, located in a preparation room at MAX IV Laboratory, is heated until 100 degrees C, and the wafers are placed on a block of metal placed at the bottom, close to the centre, which can be seen in figure 25. The PMMA film is baked for 2 hours, to completely solidify the film, and once removed from the oven, allowed to cool to room temperature. [25]

3.1.4 Etching

The etching process refers to the process of etching away the SiO_2, to separate the Si wafer and PMMA. The point of this step is to break the adhesion between wafer and 2D material and carry over the 2D material onto the PMMA film. [25] A 2M NaOH solution is prepared in a glass bowl and placed under ventilation. A magnetic stirrer paced at 60 rpm is used in order to circulate the NaOH solution, which is kept at room temperature. As seen in figure 26, the silicon wafers with the PMMA film is lowered into the solution using a plastic sieve. The wafer is left for 12 hours, after which it is seen that the PMMA film has been etched away from the silicon wafer, see figure 27. The silicon wafers and PMMA films are rinsed in water and dried using pressurised air at low speed, see figure 28, to ensure that they are dried properly. Once the PMMA has been etched from the Si wafer, the flakes are stuck to the PMMA at the surface of the bottom of the PMMA. The

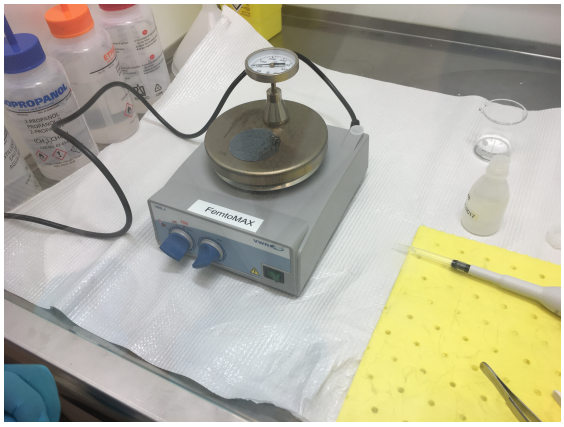

Figure 24: The solidification of the PMMA on the wafer. A total of 4 layers of PMMA is applied to achieve the desired thickness.

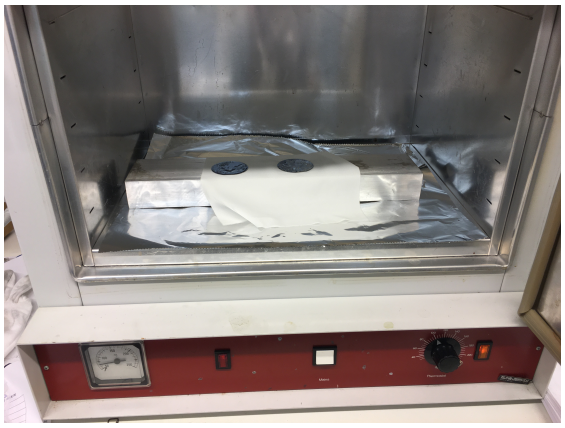

Figure 25: The PMMA film is baked for 2 hours in an oven.

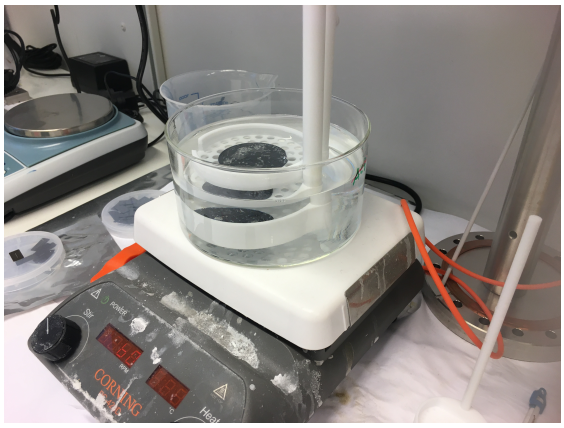

Figure 26: The NaOH solution is stirred using a magnetic stirrer and the wafers with the PMMA film is lowered with a sieve.

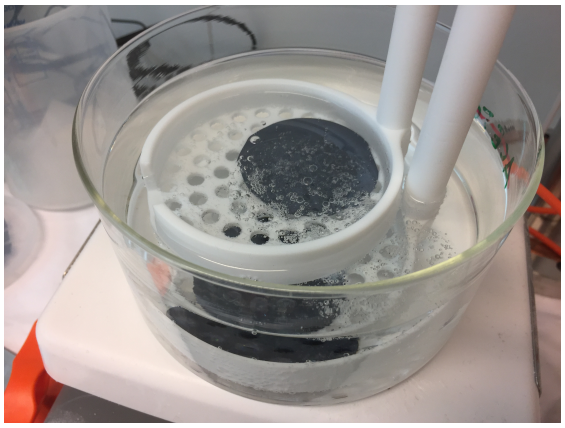

Figure 27: After 12 hours, the PMMA film has been etched from the wafer and can be seen floating in the solution.

PMMA itself is very brittle. It can be moved around without any issue, both by hand and with tweezers. Due to the brittle nature of the PMMA, one had to be careful while cutting out smaller pieces, to avoid cracks appearing.

3.1.5 Transfer from PMMA to grid

In order to transfer the flakes of 2D material from the PMMA film, they are first identified using a microscope. The process of searching and finding is made easier by using a simple ink pen, which was used to divide the PMMA film into smaller areas, as this creates reference points when using the microscope. This is shown in figure 29. In this figure, it can be seen that this particular PMMA has exfoliated graphite, as noted by the G at the top, and one half has graphite exfoliated 8 times, and the other 7 times. On the left side, a small circle can be seen, which encircles a flake of interest. In figure 30, which is an image taken with a microscope at 5x zoom, shows a flake of graphite and to the left, the blue ink is visible. In this way, it is easy to navigate on the PMMA film in search of flakes and later finding them again. The ink itself does not change the process of dissolving the PMMA, as it was readily dissolved in acetone.

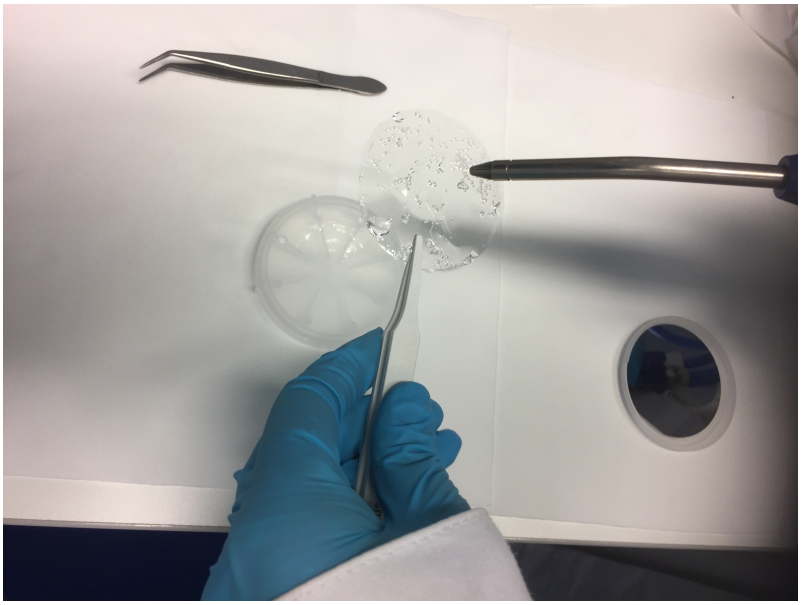

Figure 28: The wafers and PMMA films are dried gently with pressurised air.

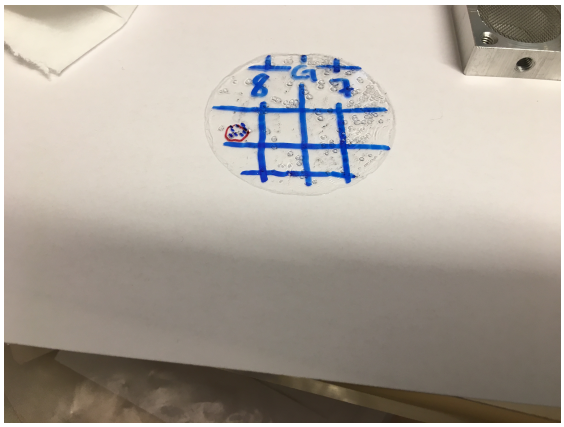

Figure 29: Simple squares are drawn on the PMMA using a permanent marker, which makes locating and refinding flakes easier.

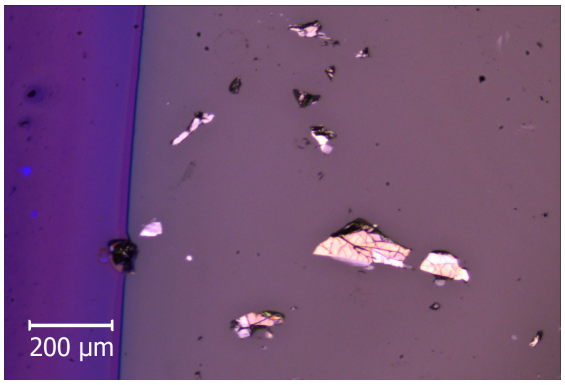

Figure 30: A flake of graphite on a PMMA film as seen through a microscope. To the left the blue ink can be seen, which is used to locate flakes on the film.

With a flake of interest located and marked on the PMMA, a piece of around 1 cm^2 is cut out, see figure 31. The cut out PMMA is then placed on a special constructed sieve. The sieve deconstructed can be seen in figure 33. The sieve was designed by the author. From the top left corner clock-wise, there is the upper lid, the upper net, the handle, a screw to attach the handle, the bottom and four screws to attach the top and upper net to the bottom. The sieve part constructed is shown in figure 34 from the top. At the side is a small hole for the handle to be attached, which can be easily rotated around the screw. The cut out PMMA is therefore placed on the bottom part in figure 32 This sieve was constructed due to the desire to be able to more easily transport PMMA, and also allow for easier dissolving by having a flat sieve that minimises movement. This sieve was built after the aluminium cradles previously used proved to move around both PMMA and grids, which caused none of the flakes to remain on the grids.

Once the PMMA is cut out, a grid is placed over the flake. To ensure that the grid is properly secured to the PMMA, evaporation of water is used. First, a water drop is placed over the PMMA,

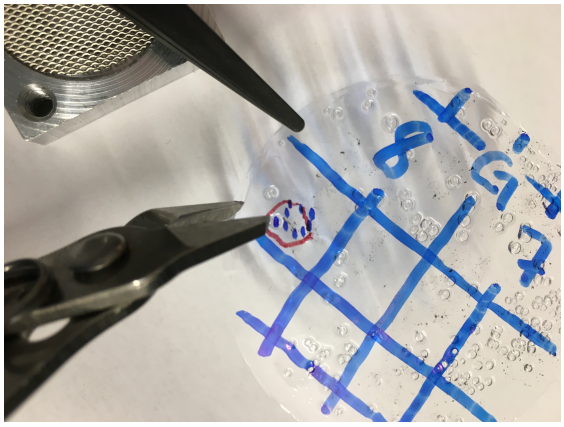

Figure 31: With a flake of interest located, a piece of PMMA is cut out.

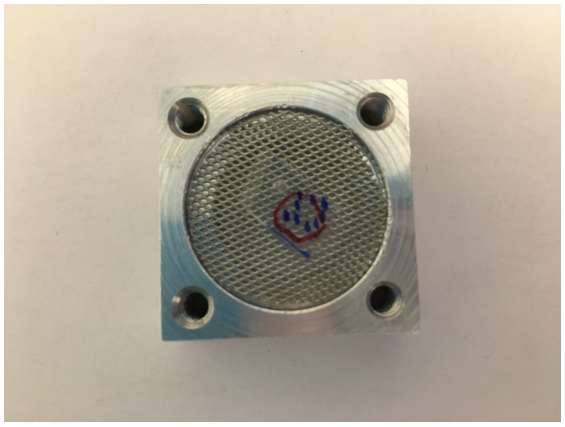

Figure 32: The PMMA is placed on the sieve built for this project.

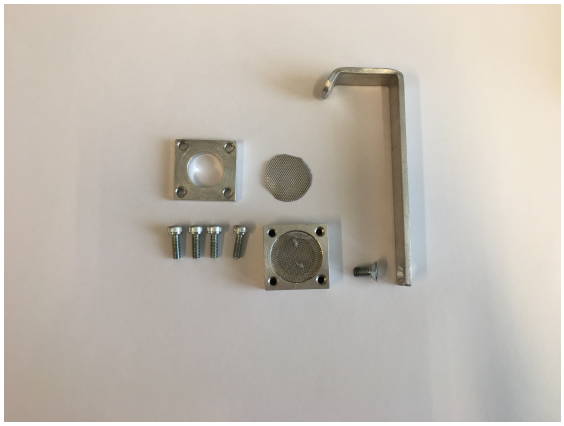

Figure 33: The sieve deconstructed.

Figure 34: The sieve part constructed.

as shown in figure 35. The drop of water is dome shaped due to the surface tension, figure 36 and in order to break this a small tissue is used as seen in figure 37, which breaks the surface tension and allows the water to be distributed more evenly over the PMMA, as seen in figure 38.

Next, the grid is placed over the water. The grids used can be seen in figure 39, which are copper grids from Ted Pella. [32] The grids are of model G600HSS, which are 3.05 mm in diameter, a hole width of 37 µm, bar width 5 5 µm and a transmission of 78 %. The grids have one smooth side and one rough side. The smooth side is described as flat and can be seen in a microscope to be more shiny when compared to the rough side. The rough side can be likened to a sandpaper. While there is some debate over the usage of either side of the grid, in this project the rough side is utilised. This decision was made with the reasoning that the sample prepared have a rough surface, due to the exfoliation method used, and the smooth surface would allow for lesser contact area than another rough surface [33]. The flake is carefully placed using tweezers, and as the surface tension is broken, the grid can be easily moved until it covers the flake. A grid placed over a flake of BP can be seen in figure 41.

Once it has been confirmed that the grid is placed correctly, the drop of water is allowed to evaporate. By using this method, the evaporation pulls the PMMA and grid close enough to allow the atoms to form bonds of van der Waals character, which ensures that the grid remains in place. [25] Due to the construction of the sieve, the PMMA and grid were left on it, as seen in figure 42

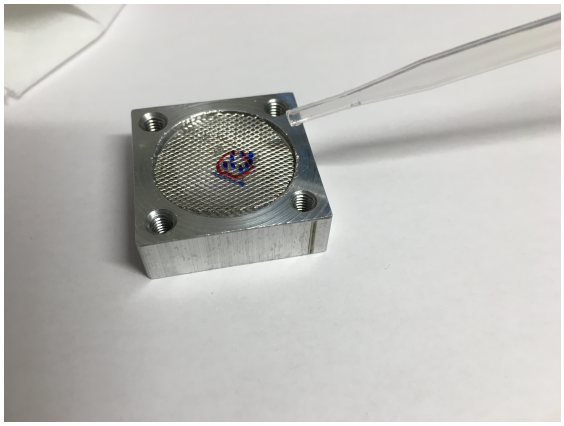

Figure 35: A water drop is applied to the PMMA with a pipette.

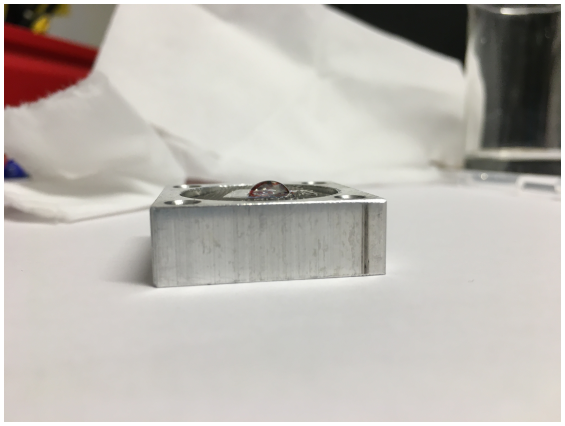

Figure 36: The water drop as seen on the PMMA. The surface tension keeps the drop in the shape of a dome.

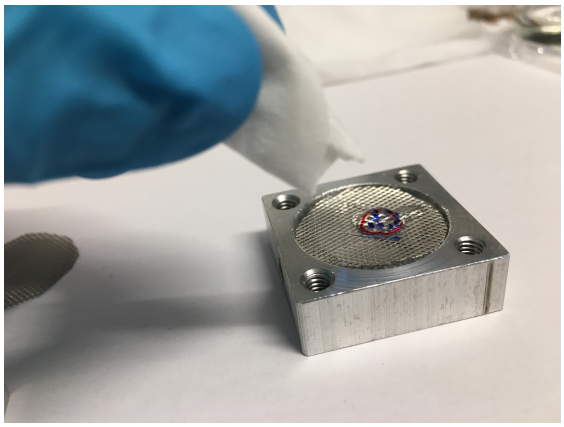

Figure 37: A small tissue applied to the water drop with the purpose of breaking the surface tension of the drop.

Figure 38: With the surface tension of the water drop, the water spreads over the PMMA more evenly.

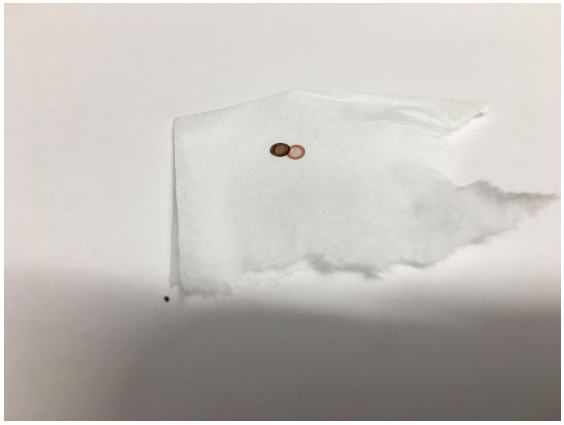

Figure 39: The Ted Pella copper grids used.

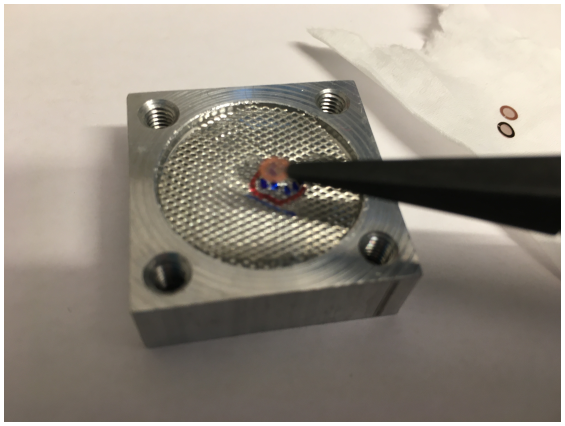

Figure 40: Using tweezers, the grid is placed over the flake.

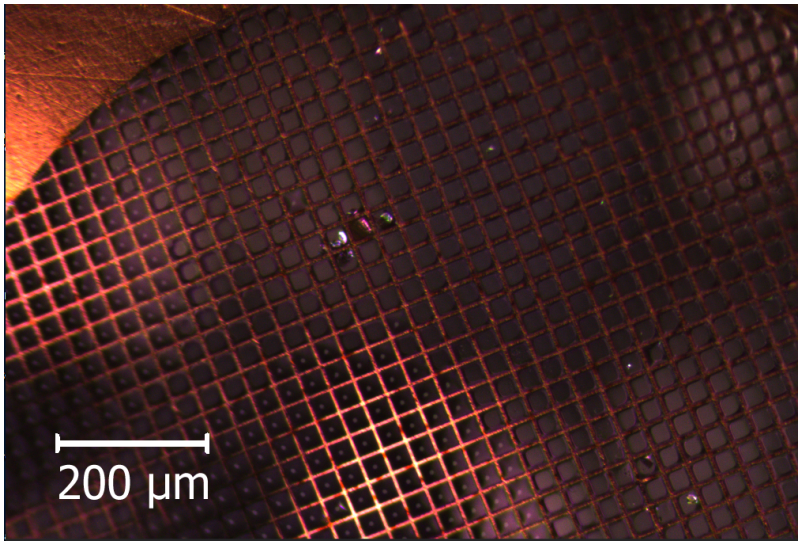

Figure 41: A flake of black phosphorus below a grid. The size is 150 µm × 70 µm.

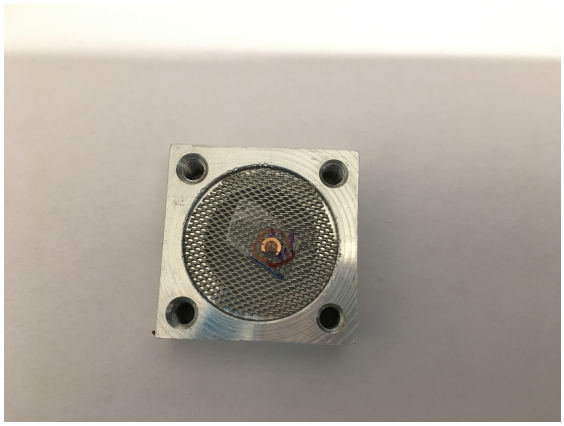

Figure 42: The grid placed on the PMMA, which is placed on the bottom part of the sieve.

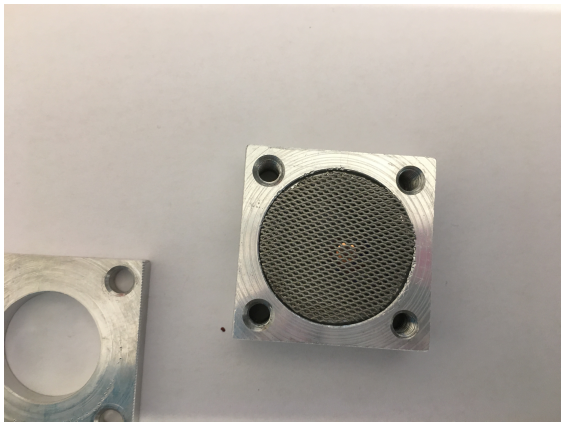

Figure 43: The upper net is placed over the PMMA and grid.

and the upper net is placed over, as it was noted that allowing the PMMA and grid to dry under a weight allowed better adhesion. Once the drop has completely evaporated, the lid is screwed in place. In the process of applying the grid to the PMMA, the PMMA is kept at the bottom for practical purposes, as shown in figure 44. However, for the process of dissolving the PMMA, it is preferable to have the grid at the bottom, and the flake and PMMA on top. Due to the nature of the sieve built, this is easily fixed by turning the sieve upside down, see figure 45 as the handle can be screwed on in any angle around the axis of the screw.

3.1.6 Dissolving of PMMA

To dissolve the PMMA film, Gonçalves et al reported using toluene [25]. However, due to health concerns regarding toluene [34], it would be preferable to use another solution. There are many solution which can dissolve PMMA [35], and other groups reported using acetone [36]. As the dangers to health are not as concerning for acetone as they are for toluene, this was chosen to dissolve the PMMA. The PMMA film with attached grid is lowered into acetone until the PMMA

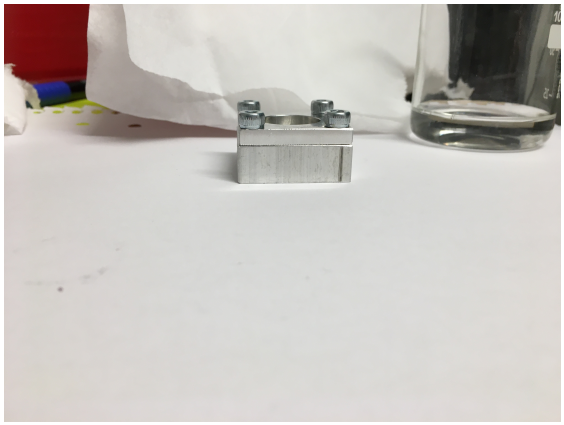

Figure 44: From the bottom: PMMA, flake and grid.

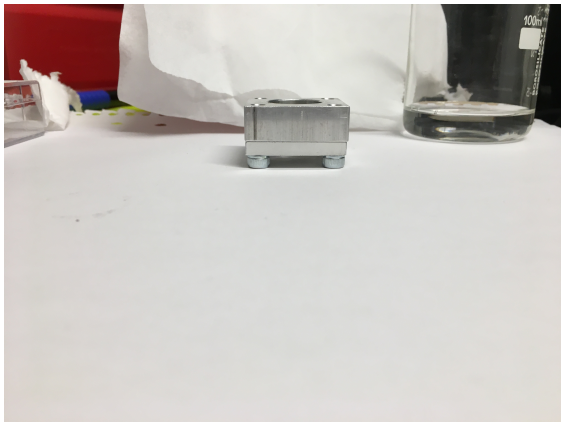

Figure 45: From the bottom: grid, flake and PMMA

had dissolved completely. For this step, the goal is to dissolve PMMA and leave the grid with the BP flakes. For the solution, different ratios of acetone to water is tested: 100 % acetone, 75 % acetone to 25 % water and 50 % acetone to 50 % water. Once the flake have been successfully transferred to the grid, this concludes this specific method to prepare samples.

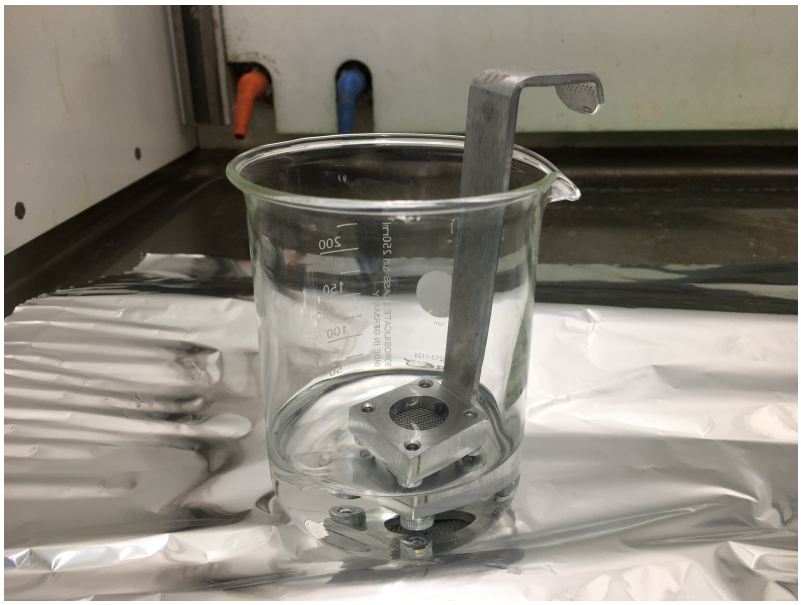

Figure 46: The sieve lowered into an acetone solution.

3.2 Transfer flake of 2D material to grid from solution

Another approach to prepare samples was also tested, which involved testing the potential of using pre-prepared flakes of black phosphorus, bought from a manufacturer. A bottle of Monolayer Black Phosphorus Solution from 2D semiconductors is used, where the solution of ethanol contained pre-prepared single and few layered BP. [37] The flakes found in this solution are exfoliated by ultrasonic treatment and are diluted in ethanol. As the solution is supersaturated, it is recommended to dilute with ethanol, and the recommended ratio can be seen in table 3. The size of the flakes in this

solution range from 25 nm to 10 µm according to the documentation, and the number of layers are 1 to 10s of layers and the surface is reported to be smooth.

BP solution (ml/number of drops)	Ethanol (ml)
0.05/1	6.25-12.5
1/20	125-250

Table 3: The recommended ratio between the supersaturated black phosphorus solution and ethanol. [37]

3.2.1 Pouring solution over grid

In order to enable dropping solution over a grid, two metal plates of aluminium were constructed. These were built for the purpose of keeping the grid in place and allowing the solution to have somewhere to drain. The deconstructed plates can be seen in figure 47a along with two vices used to press the plates together. One plate has a hole with a diameter of 2 mm, which is smaller than the grid, which is 3.05 mm [32], and the other plate has a hole with larger diameter, 5 mm. When the plates are pressed together, this creates a funnel which allows liquid to pass through the funnel unhindered. A top view of this set up with the two vices used to secure the two plates together can be seen in figure 47b This funnel creates a slot for the grid, where it can be locked into place to ensure that it does not move during the transfer process. The grid is placed over the smaller hole, as seen in figure 48a, with the other plate placed on top, as seen in figure 48b

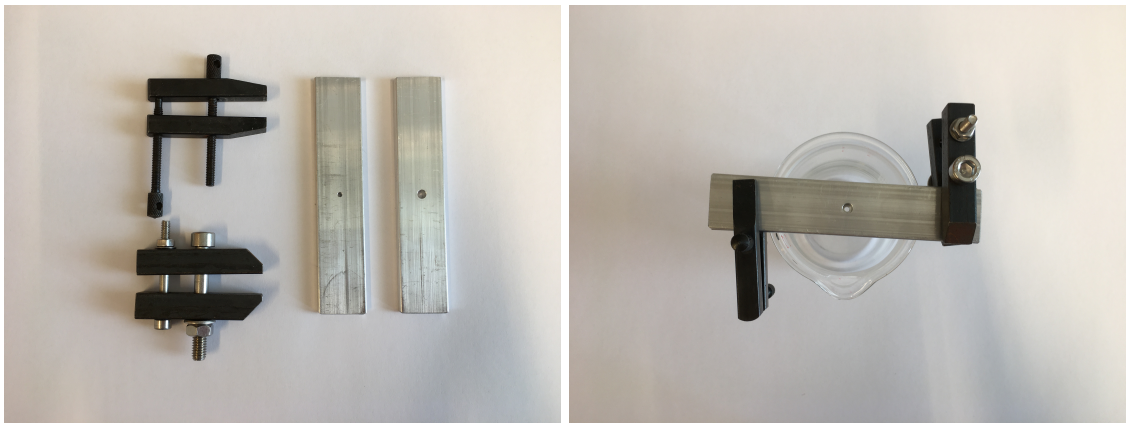

(a) The metal plates, one with a hole of 2 mm diameter and the other with 5 mm, as well as two vices.

(b) The assembled product. The two vices are used to press the two metal plates together.

Figure 47: The aluminium plates, deconstructed and constructed.

The plates are then placed over a beaker, to gather the drained liquid. Another beaker was prepared with the BP solution diluted as in table 3. By using a pipette, this solution was slowly dropped over the grid. Another attempts is made with drops directly from the bottle as seen in figure 49. The grids are then examined in a microscope to see if any flakes are present. The beaker and metal plates are kept under a fume hood.

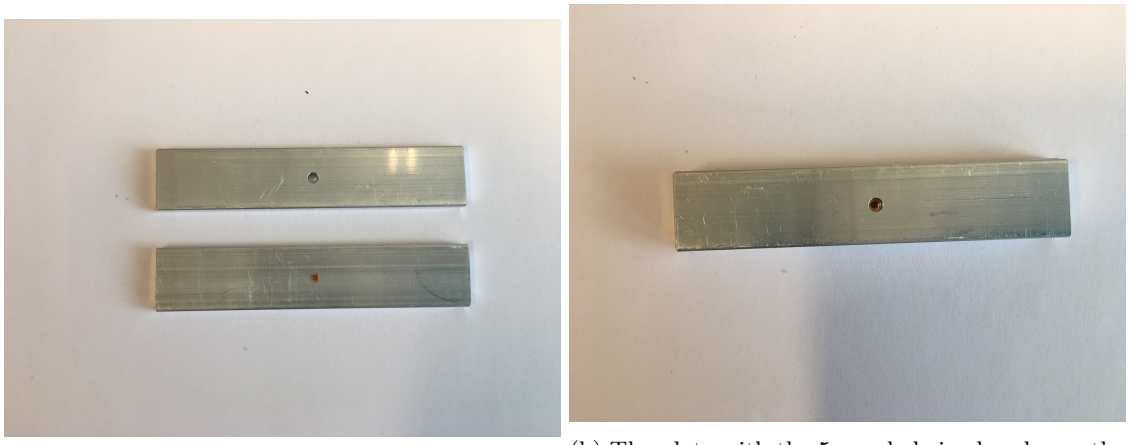

(a) The grid is placed over the hole of 2 mm.

(b) The plate with the 5 mm hole is placed over the grid. The grid can be seen in the hole.

Figure 48: The principle of the metal plates and placement of the grid.

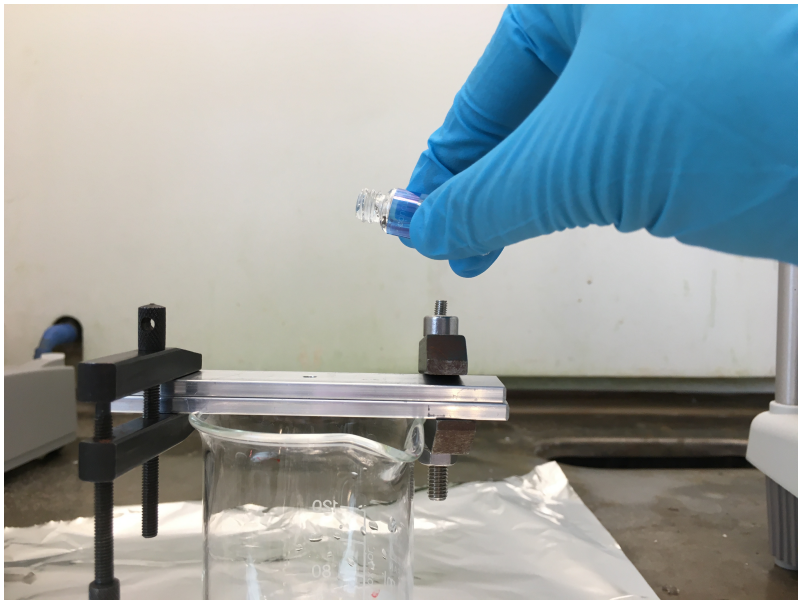

Figure 49: The metal plates placed over a beaker, and solution is dropped from the top.

3.2.2 Dragging grid through solution

A solution is prepared with the ratio shown in table 3. A pair of chemically resistant reverse type tweezers is used to grad one grid by the edge. [1] This allows the grid to be held firmly without risking to apply to much pressure, which could cause the grid to bend or break. The grid is dragged through the prepared solution as a net, as seen in figure 50 in order to examine if this is a valid method of catching flakes on the grid.

[1] A normal type pair of tweezers is open as status quo, and when pressure is applied it closed, and a reverse type is the other way around, so that is is closed normally and opens when pressed.

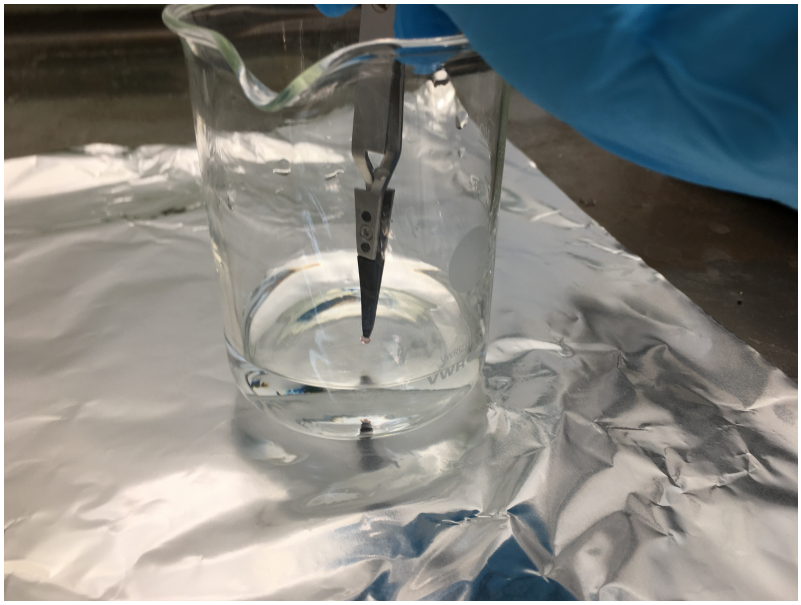

Figure 50: A grid held by a pair of reverse type tweezers, slowly moved through the solution.

3.3 Sample orientation

In order to identify the orientation of a BP sample, polarisation dependence of the Raman peaks can be used, which can be seen in figure 10. A laser of wavelength 532 nm is absorbed by the sample, and the spectrum is measured by a spectrometer, which depending on the peak chosen, displays a different polarisation dependence. The set up is shown in figure 51. The arrows indicate the direction of the laser light. The laser passes through a half-wave plate, located at the letter A in the figure and then a polariser (letter B). With this, the polarisation of the light can be controlled, and with the half-wave plates the power of the incident laser is moderated. Due to the set up, horizontal light is seen when the polariser is turned to 290 degrees. After the polariser, the laser is sent to the sample, and the Raman signal then passes through a second polariser (letter C) and a second half-wave plate (letter D) before finally ending at the spectrometer. This second set of polariser and half-wave plate allows for control of parallel or cross polarised signal. Parallel polarised light occurs when the polarisers placed at the incident light and the reflected light are rotated to the same orientation, and cross-polarised is the result of the polarisers rotated perpendicular in respect to each other. Due to the two polarisers introducing a slight angle shift, the entrance slit of the spectrometer is set to 700, and the grating is set to 150 g/mm, which decreases the resolution, but allowed the peak of the A_g^1 mode to be resolved. For this particular peak, it can be seen in figure 10 that the highest intensity of the parallel polarised light corresponds to the ZZ-direction. The lowest intensity, the AC-direction, is acquired when the rotation of the polarised light has changed by 90 degrees. For cross-polarised light, both the ZZ- and AC-direction corresponds to minima. [24]

3.4 Sample thickness

To calculate the thickness of a sample, the absorption of the sample of BP is measured and the Beer Lambert equation 6 is used to calculate the thickness. The thickness is estimated after transferring the BP flake to the copper grid.

As the absorption of the sample itself is difficult to measure, the ratio of the intensity of the BP

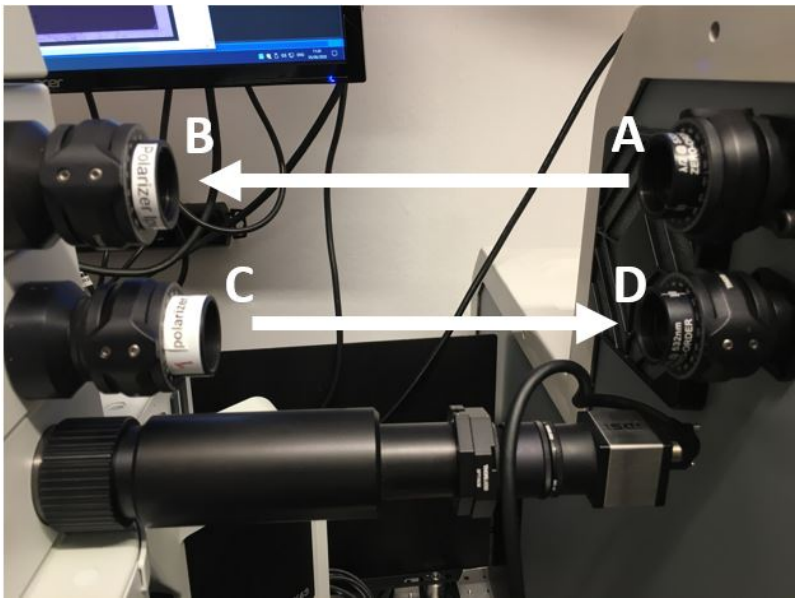

Figure 51: The laser of wavelength 532 nm travels along the arrows indicated in the figure. The letters A and C represents polarisers and B and D half-wave plates. A and B controls the polarisation of the light before the sample, and C and D controls the polarisation of the Raman signal before being measured with the spectrometer.

sample is divided by a reference signal. To do this, the sample is placed onto a clean silicon wafer. A laser, of wavelength 532 nm, is directed onto the silicon surface, and the Raman scattered spectrum is measured using a spectrometer. The set up is as shown in figure 51, where the incoming laser first passes through a half-wave plate (placed at the letter A in the figure) then through a polariser (letter B). This ensures that the sample is only exposed to one polarisation at a time, as there is a polarisation dependence of the absorption. Once the laser is absorbed by the silicon wafer, the Raman spectrum is measured using a spectrometer, and the intensity of the Raman signal from the 521 cm^{-1} vibrational mode of Si is recorded, as is shown in figure 9. The spectrometer is set to 10 seconds exposure time, with an entrance slit of 100 µm and grating with 300 grooves per mm is used. The intensity of the Raman signal of silicon is first measured for horizontally polarised light, then the measurement is repeated for a range of 110 degrees in steps of 10 degrees.

After the reference value from silicon is acquired, the laser is directed onto the BP sample mounted on the silicon wafer, and the same method is repeated, for the same orientations of the polariser. By dividing the signal intensity of the sample of BP mounted on the silicon wafer with the intensity of the signal from the silicon wafer, a maximum and minimum is acquired. The maximum ratio corresponds to the lowest absorbed direction, which in turn corresponds to the ZZ-direction and the minimum ratio then corresponds to the highest absorption, the AC-direction. For the wavelength of the incoming laser, 532 nm, the corresponding energy is 2.33 eV. Ling et. al [22] have measured the anisotropic Raman scattering intensity for three different wavelengths (532 nm, 633 nm and 785 nm) for four different thicknesses (˜5 nm, ˜20 nm, ˜40 nm and ˜200 nm), as well as values of absorbance for two different thicknesses, 9 nm and 225 nm. By comparing the measurements performed in this project to the measured values of Ling et. al., and approximate thickness of the BP sample can be calculated. Values from the thickness of 225 nm is assumed. By using the relation $A = \log_{10}(T)$, the transmission T is calculated to be 0.0776 for the ZZ direction and 0.224 for the AC direction. By inserting the assumed thickness from Ling et. al. into the Beer Lambert equation (6), the absorption coefficient can be calculated. Then, the maximum and minimum ratio between the measured intensity from BP and reference Si is corrected for the internal reflections of the sample. For refraction between materials of refractive index n_1 and n_2 and incident angle 0

degrees, the amount of reflected light is given by $\frac{n_1-n_2}{n_1+n_2}$, with the amplitude given by $R = (\frac{n_1-n_2}{n_1+n_2})^2$. The intensity of the reflected light is then $T = 1-R$. [38] The refractive index n for air is 1 and for BP, it is 2.6 for the AC direction and 3.1 for the ZZ direction. [39] For the incident laser, a loss of intensity is made from reflection from the transitions between different materials. This gives a total of 30 % of signal loss for the ZZ direction and 41 % for the AC direction. By reinserting the value of the absorption coefficient in the Beer Lambert equation (6) together with the ratio between the highest and lowest intensity, corrected for the loss of intensity, an approximate thickness z of the sample can be calculated. A full walk through of the calculations can be seen in appendix A.

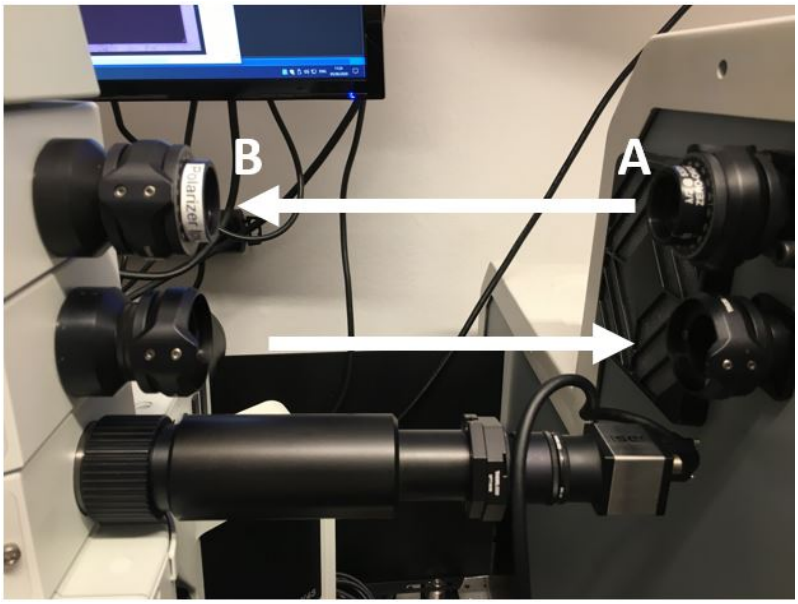

Figure 52: The set up to control the polarisation of the 532 nm laser. A represents a half-wave plate and B a polariser. The arrows indicates the direction of the laser light.

4 Results and discussion

4.1 Effects of different number of exfoliations and differences between graphite and BP

As would be expected, a higher number of exfoliations leads to laterally smaller flakes. As can be seen when comparing the flakes of the two materials on a PMMA film in figure 53a and 53b, figures which were chosen to be as representative of the general results as possible, it can be seen that the flakes of graphite has a larger area than that of the BP. It can also be seen that BP has a slightly higher tendency for small fragmented flakes close to the larger flakes. This can have several explanations. This can be dependent on the structure of the layers in the material, as was seen in figure 3 for BP and figure 2, as graphite has flat layers, whereas BP has a puckered structure. The symmetry of graphene means that every atom has an equal force contributed by the surrounding atoms, but for BP the surrounding atoms are not in a plane, which changes the angle between bonding of the in-plane structure. This could cause more angles of attack for the BP structure which could cause the higher likelihood of smaller fragments. However, this could also be due to the quality of the initial bulk material, and whether the initial structure is free from contaminations of other materials and the structure does not have any weak points. There is also the effect of the exfoliation process itself, were the adhesive material might not be applied evenly, or any dry spots with less effect. There was not found to be any differences between the speed of exfoliation, however this does not necessarily mean that there is no dependence on this.

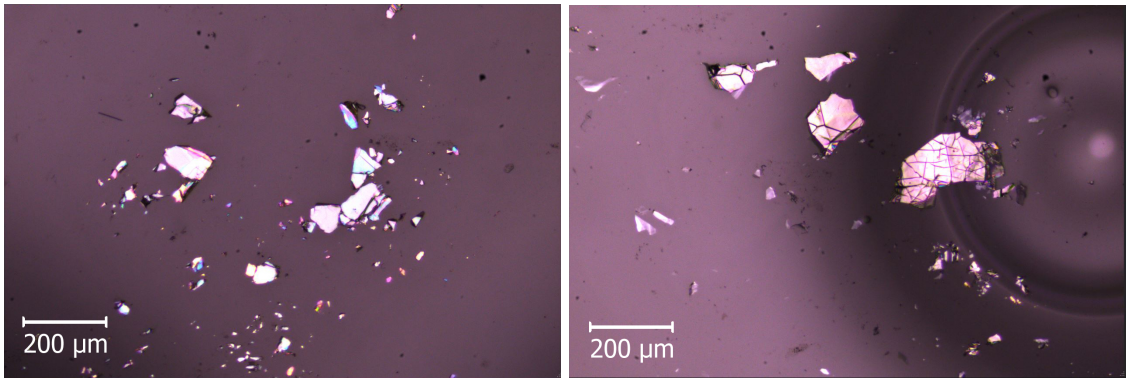

(a) Black phosphorus (b) Graphite

Figure 53: Total of 7 exfoliations on PMMA as seen through a microscope.

The thickness of the initial exfoliation is also of importance, as thicker layers would be more likely to contribute to larger area of flakes. As a continuation to the adhesion of the tape, it can also be noted that there is no guarantee to always divide the existing flakes in half when exfoliating, which means that a certain number of exfoliations does not immediately corresponds to a certain thickness.

Between figure 53 and 54, the number of exfoliations has increased by one, which causes the flake area to decrease for both materials. The general behaviour remained the same as for 7 exfoliations, with the addition that in some areas, graphite stated to show more smaller fragments, while still not as common as for BP.

In figure 55, 9 times exfoliated BP can be seen, which shows the expected behaviour of smaller fragments surrounding larger flakes. The area of the flakes are indeed smaller that in figure 54a, and fragmentation can still be seen.

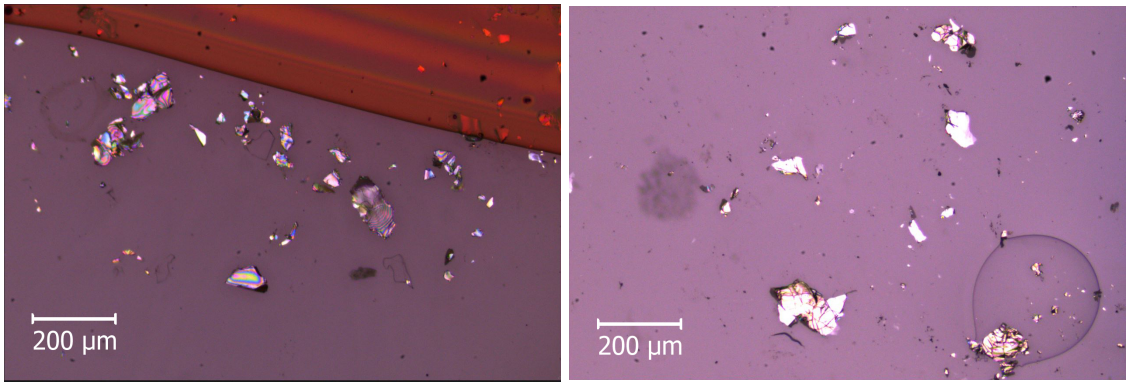

(a) Black phosphorus (b) Graphite

Figure 54: Total of 8 exfoliations on PMMA as seen through a microscope.

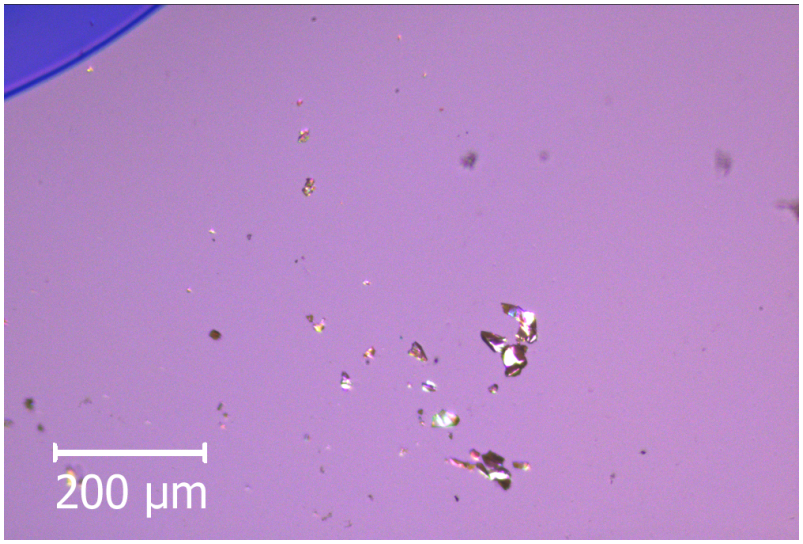

Figure 55: Black phosphorus with a total of 9 exfoliations on PMMA as seen through a microscope.

4.2 Importance of hotplate

As described in the method, the effect of using a hotplate to melt the adhesive before peeling of the tape from the Si wafer was compared to the results from not using a hotplate. The results can be seen in figure 56a and 56b. The effect of the hotplate is clear, as without using the hotplate there were no larger cohesive flakes seen at all, instead all flakes were fragmented into too small flakes to be of interest. This leads to the conclusion that the adhesion of the tape to BP and graphite is stronger than the adhesion between graphite and BP to the Si wafer. Therefore, to provide the best results of this step, a hotplate should be utilised to melt the adhesive before peeling of the tape.

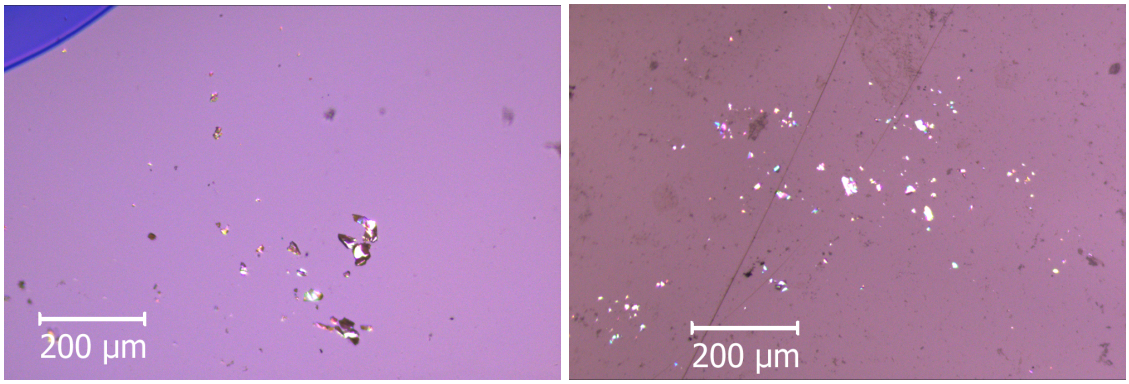

(a) Hotplate used to melt adhesive of tape.

(b) Hotplate step skipped.

Figure 56: Black phosphorus flakes on PMMA, exfoliated 9 times.

4.3 PMMA and the transfer process

4.3.1 Applying copper grid

For the process of adhering the copper grid onto the PMMA film, it was seen that the adhesion was not as easily performed as described in the litterature. The effects of surface tension on the drop of water applied to the PMMA was tested.

In the method section, 36 shows the dome shape of a water drop, and this dome shape is caused by the surface tension. When applying a copper grid to the water dome, the grid readily moved to the top of the dome, which made the placement of the drop crucial. However, it was found that breaking the surface tension allowed for easier aligning of the copper grid with the flakes in the PMMA film. By breaking the surface tension, the water spread more evenly over the PMMA film, which made it possible to adjust with the help of an optical microscope. Surface tension also increased the evaporation time. A drop of around the same volume with surface tension would lead to an evaporation time of close to 2 hours, whereas a drop were the surface tension had been broken would take around 1 hours to evaporate. It was also noted that the van der Waals bonding created between the copper grid and the PMMA film was sensitive to shear stress, which meant that any applied force along the surface of the grid would cause the grid to loosen.

4.3.2 Dissolving PMMA

The dissolving process proved to be the most time consuming step, as there were several complications introduced in the process of making sure that the flake of 2D material would remain attached to the grid. The initial test saw that acetone did indeed dissolve PMMA, and did so within 15 min, as seen in table 4. During the first tests, the PMMA with the attached grid were lowered into the solution using a simple cradle of aluminium foil, which saw the acetone completely dissolving the PMMA and also allowing the grid to come out clear, without any 2D material left. The time to completely dissolve PMMA is dependent on concentration and type used, and the table shows the results.

Initial tests showed that acetone indeed dissolved the PMMA, but the BP flake was also lost in the solution instead of remaining attached to the grid as desired. The purpose of reducing the concentration of acetone was to test if the acetone concentration was the cause of losing the 2D material flakes in the first tests. For the 75 % and 50 % acetone solutions, the problem of

Acetone/water	Time to dissolve PMMA
100/0	15 min
75/25	around 4 days
50/50	6+ days

Table 4: Time to dissolve PMMA.

evaporation was then introduced as the solution had to be left for several days. This meant that the solution had to be refilled, which introduced two problems: the uncertainty of the ratio after refilling and turbulence in the solution introduced by the refilling process. However, after several attempts of different ratios, it was concluded that the introduced turbulence was the most likely cause of the lost flakes, as the adhesion of the 2D material is most likely stronger than the adhesion between 2D material and grid. The dissolving process starts with the exposed PMMA, which means that the PMMA close to the grid most likely was dissolved before the flakes of 2D material were completely released from the PMMA, which caused the PMMA to drift away with the flakes.

One test allowed the grid to remain in the beaker in a 100 % acetone solution until the acetone had completely evaporated, however this left a thin film of PMMA residue across the beaker as well as the grid, leaving it unusable.

The conclusion from these tests are that the adhesion between 2D material and grid is not strong enough to withstand the dissolving process without aid. The turbulence of the liquid has to be decreased , and the grid with the PMMA film should remain as still as possible during the entire process of inserting, dissolving and retrieving from the solution.

4.3.3 Sieve

With these factors in mind, a flat sieve, as described in the method, was constructed. This sieve served multiple purposes. First, it allowed the cut-out piece of PMMA to be left undisturbed as much as possible in the process of transporting and storing the sample, which decreased the likelihood of damage. Secondly, it held the grid and PMMA in place when moving in and out of the acetone solution, and the holes of the sieve allowed circulation of PMMA and acetone evenly in all directions and also allowed the grid to dry once out of the solution. Thirdly, the flat construction allowed the grid to remain as undisturbed as possible.

4.3.4 Air bubbles

When applying the PMMA, air bubbles were not uncommon. These bubbles were most likely formed due to the fact that the PMMA solution was applied with the Si wafer placed on a hotplate, and the application process, in which the pipette used most likely introduced air bubbles. As the solidification process of the PMMA is started as soon as it comes into contact with the heat, the PMMA with the encased air bubbles is solidified. A typical example of air bubbles can be seen in figure 57, and since the PMMA is solidified onto the Si wafer, air bubbles does not cause the surface containing the 2D material to change in any meaningful way, as it remains flat. It does however cause a problem if, as seen in figure 58, there is a flake of a desired size and shape. Air bubbles were noted to cause the dissolving process of PMMA to become even more uneven. Therefore, it was concluded that any flakes close to an air bubble would have a higher likelihood of not becoming stuck to the grid and they are best avoided.

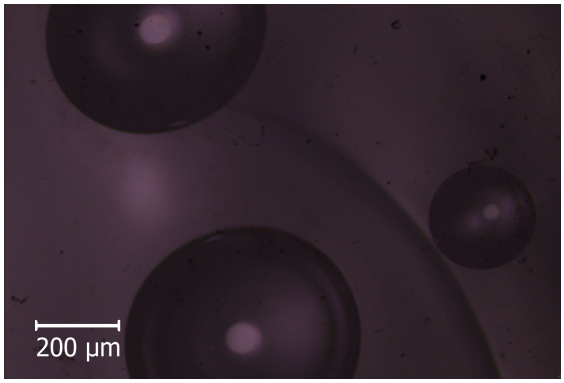

Figure 57: Air bubbles in the PMMA film as seen through a microscope.

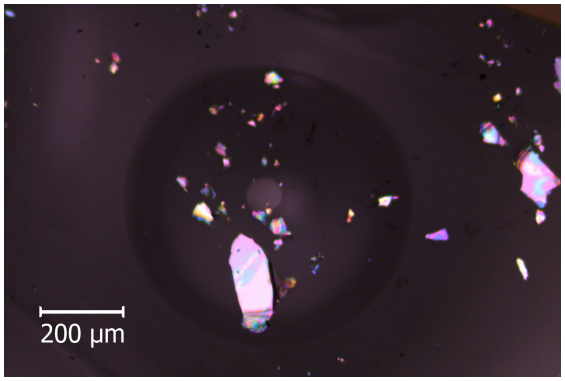

Figure 58: Air bubble in the PMMA film and a flake of BP.

4.3.5 Adhesion of flakes

It was found that once the flakes had been properly transferred onto a new substrate, it was very likely to remain in place. This was apparent in the process of cleaning the Si wafer in acetone from the tape residue after hotplate usage, as most of the adhesive was dissolved, but the BP and graphite remained. This was also apparent on the flakes that were stuck onto the copper grid. Grids with flakes were bent and dropped from a height of 1 m to test this, and while this caused damage to the grid, the flakes would remain.

4.3.6 Successful transfer from PMMA to grid

By using the sieve, several flakes were successfully transferred to the copper grids. Three different transferred flakes of BP can be seen in figure 59, 60 and 61. For all figures, the focus is uneven, which is due to the grids being very thin and sensitive, and movement while they are not yet dry usually caused a slight bend in the grid. The flake in figure 59 appears to be somewhat transparent, which could be a sign of the flake being thinner that other flakes found. The rainbow colouration most likely indicates varying thickness of this particular flake. The flake seen in figure 60 appears to be thick and the surface appears similar to that of a bulk of BP. In figure 61, three flakes are seen close together. The flake which is in focus is around 90 µm × 40 µm, and the surface appears to be flat. When comparing this size to the electron beam for the set up, 200 µm in diameter, the size of this flake is around 10 %. This gives a decent probability of seeing electron diffraction. This flake was chosen for further testing. Due to degradation of BP in ambient conditions, the sample was stored in vacuum in between experiments.

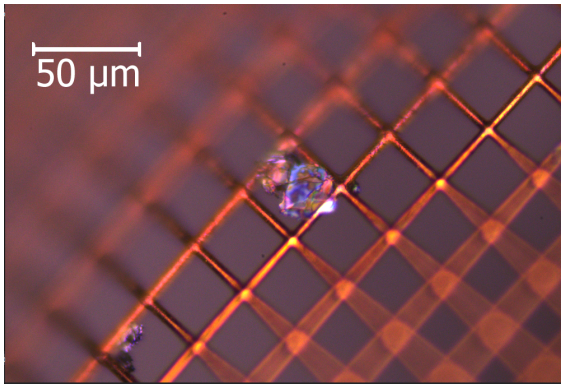

Figure 59: A 50 µm × 50 µm suspended flake of BP.

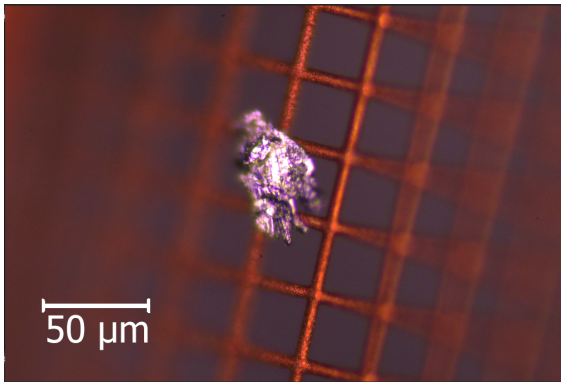

Figure 60: A 100 µm × 50 µm suspended flake of BP.

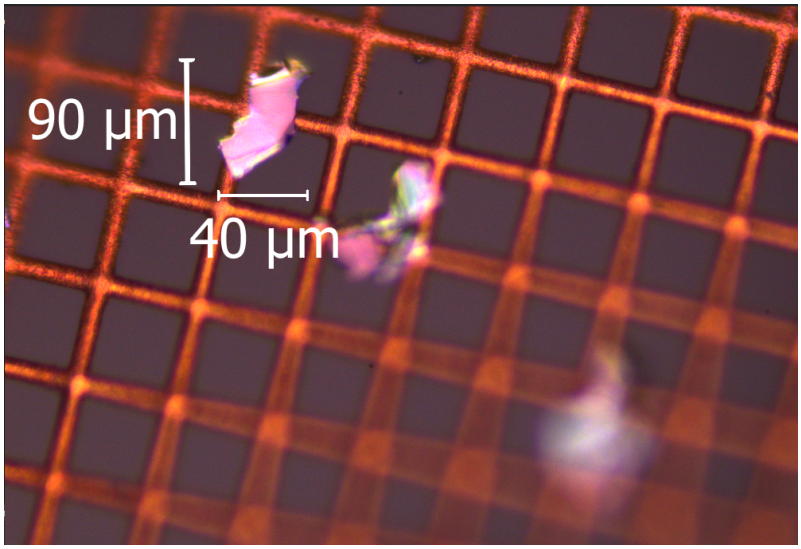

Figure 61: A 90 µm × 40 µm suspended flake of BP, with two other flakes out of focus of similar size.

4.4 Black phosphorus from solution

4.4.1 Pouring solution over grid

The method of pouring solution over a grid directly did not yield a successful result. The first concern was whether the bars of the grid were spaced enough so that the solution could drop through. This proved to be unfounded as the solution dropped through without any problem. However, due to the tight spacing of the bars of the grid, the solution seeped through at a slow rate, which caused larger drops to seep in between the metal plates. The grid would remain in place, as the metal plates were pressed together tightly, however the liquid seeping out could possibly cause any BP flakes in the solution to drift.

Initially, this method of testing used a diluted solution, which was diluted according to table 3. After 20 attempts of one drop, drying the grid and examining the results in a microscope, the conclusion was drawn that this method did not work. Therefore, the method was repeated with the solution directly from the bottle, performed 10 times. This did not change the result of the

method. This can be assumed to be due to the small size of the flakes. The sizes of the larger flakes found in the solution are 20 µm × 30 µm, and can be seen in figure 62a and 62b. This means that the flakes are smaller than the holes of the grid, which is 37 µm × 37 µm, which gives a low probability of the flake adhering to a grid compared to falling through without contact with a grid. When compared to the method of transferring by use of PMMA, where the 2D material flakes are known to be positioned parallel to the grid, the orientation of the flakes of the solution in this method is unknown. If the positioning of the flake is parallel to the grid, this gives the largest possible area to adhere to the grid. If the flake is rotated compared to the grid, the area of contact becomes smaller, thereby reducing the probability of transferring a flake. Overall, the probability of successfully transferring a flake from the solution to a grid was deemed low, as a total of 30 attempts yielded 0 successfully transferred flakes, for a probability of 0 %.

4.4.2 Dragging grid through solution

With the solution mixed with ethanol, dragging a grid with the use of self-closing tweezers, some of the flakes present were stuck to the grid. It was found that a slow sweeping motion yielded the highest likelihood of finding a flake on the grid. The largest flakes caught can be seen in figure 62 and 62b. What can be seen with this method is that the flakes caught are very small and the best case observed, in figure 62 only covers around 10 % of the hole, which would not be sufficient during experiments. The more common case is what is seen in 62b, were the majority of the area of the flake would be stuck on the grid and a very small area would be freely suspended. There is also the possibility that even if the grid was moved in a what was considered slow motion, there is a possibility that the flakes were broken around the bars.

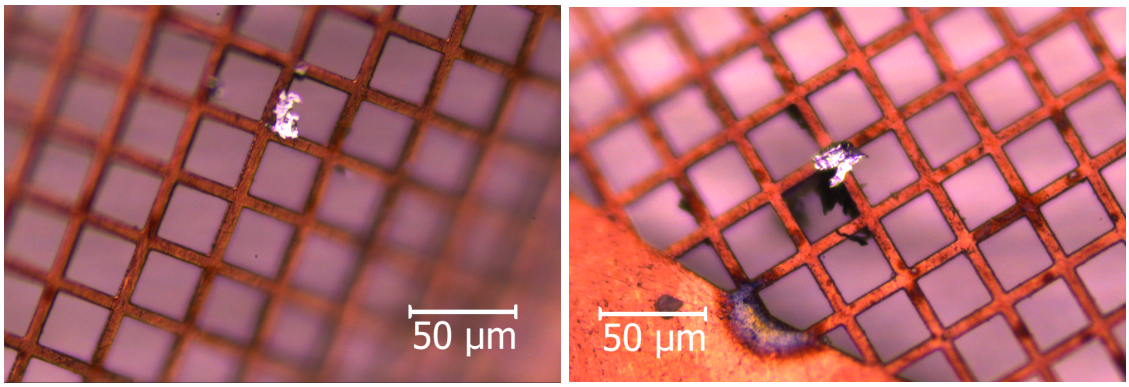

(a) The flake which was seen to be the most suspended by using this method. Around 10 % of the grid hole is covered.

(b) The typical result from the solution, the flake can be seen stuck to the bars are are mostly not freely suspended.

Figure 62: Black phosphorus flakes from pre-prepared solution.

The flakes found in this solution are too small to be of any interest, and this method caused any flakes caught to be stuck to the grids and not be completely suspended. Therefore, this method was deemed unsuitable for the purpose of suspending flakes onto a grid.

4.5 Sample orientation

The orientation measurement is seen in figure 63a for the parallel polarised measurement and figure 63b for the cross polarised measurement. For the parallel polarised measurement, the period appears to be shorter than the expected 90 degrees, however it should be noted that the peak at

120 degrees is very clear, and the minima are possibly drowned out by noise in the measurement. As the AC direction corresponds to the direction of the highest absorbance, this means that the peak corresponds to the ZZ direction, as this direction would therefore be the one that allows the most light to be reflected. The cross polarised measurement shows a more clear period, and while the second peak is lower, the period remains the same and is as expected.

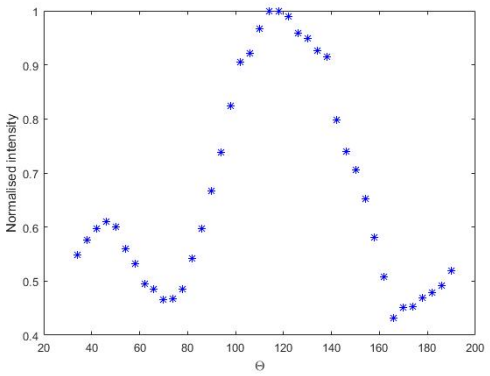

(a) Parallel polarised measurement.

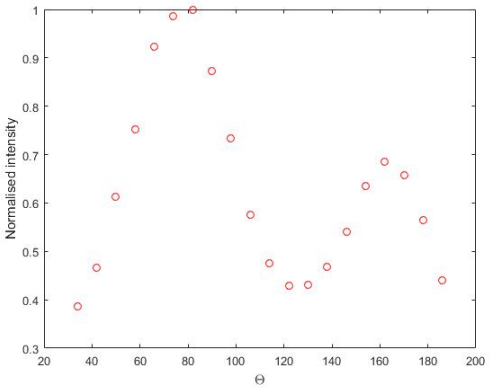

(b) Cross polarised measurement.

Figure 63: Result from the orientation measurement, performed on the same flake as seen in figure 61.

Compared to the incoming horizontal light, which is shown as the dotted line in figure 64 as well as figure 65, the ZZ direction is rotated 84 degrees anti-clockwise, as shown by the line in the same figure. The AC direction is found by rotation of 90 degrees from the ZZ direction.

It should be noted, however, that there is another flake less than 50 µm away from the target flake, as seen in figure 65. As the measurement is only targeting one flake, and there is no guarantee that these two flakes are of the same orientation, there is the possibility of interference in the signal.

4.6 Sample thickness

The thickness measurement were performed on one of the BP flakes as seen in figure 61, and the results of the measurement can be seen in table 5, with the rotation of the polariser to the left.

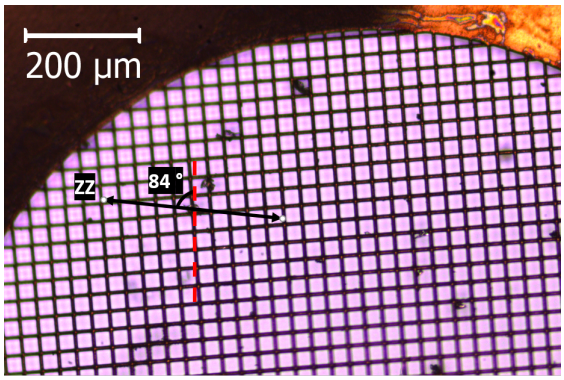

Figure 64: The placement of the flake on the grid with the ZZ direction drawn out.

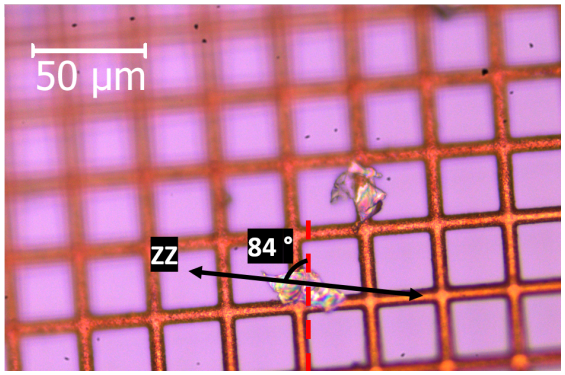

Figure 65: The placement of the flake on the grid with the ZZ direction drawn out.

The ratio between the two is to the right, as this ratio is plotted over the polarisation in figure 66. In this figure, the minimum ratio seems to be located at 310 degrees and the maximum ratio at 380 degrees. This is a difference of 70 degrees, which differs from the expected 90 degrees, but as can be seen in the figure, there is another peak at 410 degrees, which gives the possibility of the actual maximum somewhere in between these values. For the purpose of this measurement, 70 degrees is deemed to be close enough, as the limitations in how fine the polariser can be rotated by hand as limits the amount of data points possible, and as the purpose is finding an approximate value, this is deemed to be sufficient.

Polariser	Si only (counts)	Si with BP (counts)	Ratio
290	35579	7428	0.2088
300	35036	6882	0.1964
310	35021	6653	0.1900
320	35297	6991	0.1981
330	35922	7224	0.2011
340	36471	7142	0.1958
350	37518	7537	0.2010
360	38385	7967	0.2076
370	39371	8193	0.2081
380	39869	8518	0.2136
390	40204	8314	0.2068
400	39961	8178	0.2046
410	39345	8343	0.2120
420	38817	7823	0.2015

Table 5: The counts for Si with and without BP as well as the ratio between the two.

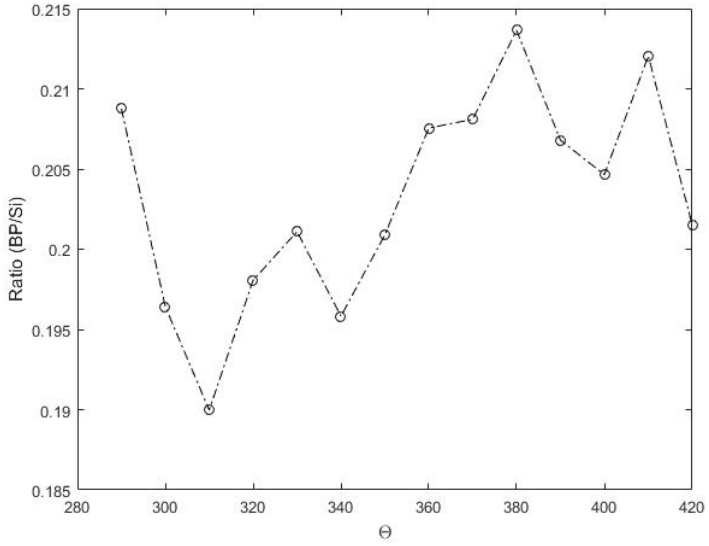

Figure 66: The ratio of black phosphorus over silicon as a function of the rotation of the polariser.

By following the method for calculating the thickness presented in the method, with the exact steps shown in Appendix A, this finally gives the approximate thickness of 33 nm for ZZ and 30 nm for AC. According to the graph presented in figure 5, this thickness is thin enough to allow electrons of incident energy 60 keV to pass through. Possible sources of error in this measurements stems from the values taken for the refractive index of BP [39] and the absorbance [22] for the different

directions AC and ZZ. The assumption of the thickness 225 nm from the values presented by Ling et. al. [22] also presents a source of error, as the values presented are experimentally measured, and as the thickness does not match the thickness of the sample prepared in this project, there will be a discrepancy in the answer due to the assumed value. The value of 225 nm was assumed due to comparisons between AFM (Atomic Force Measurements) performed on samples of down to 60 nm mounted directly onto silicon. Between 60 nm and bulk BP, the values for absorbance does not change significantly, however, if the sample is thinner these changes in the value of absorbance become more pronounced. There are also possible sources of error in the method of measuring the thickness. In the set up, two polarisers have been used, and both of these introduce a slight lateral movement of the incident laser beam. As the polarisers are rotated, this movement introduces the possibility of the laser beam illuminating different positions of the sample, and should the sample have different thicknesses in these positions, this could make identification of the AC and ZZ direction difficult. The lateral movement of the beam also lead to an increased opening of the slit in the spectrometer. A wider slit reduces the resolution and gives more background noise, which causes the measurement to become less precise. There is also the possibility of this movement causing the beam to in some cases slightly miss the entrance slit of the spectrometer. Finally, due to the sample being placed on a copper grid, which in turn was placed on a silicon wafer, there is a possibility of the sample being placed at an angle. All of these would result in the number of counts measured by the spectrometer not truly representing the actual signal strength from the peak of interest. For the calculations, the simplifications made in reflections and the interactions of light in the sample allows for an approximation of the thickness, but for a thin sample interference must be taken into account, the value from the calculation should only be used as approximation and not as definitive results. However a thickness of around 30 nm is indeed good for further experiments, as this value is below the maximum penetration depth as seen in the theory with margins, allowing for some errors in the calculations. This thickness is also thin enough to avoid the possibility of Kikuchi lines appearing. As Kikuchi lines are not the intention of future measurements, the diffusion depth presented in the theory is much higher than the thickness measured for this particular sample. This means that for future sample preparations, fewer number of mechanical exfoliations can be used, to produce sample flakes of larger size and thickness, as a larger area of a flake would prove useful in the process of aligning the incident electron beam with sample.

5 Conclusion

The method as presented by Gonçalves et. al. [25], was found to successfully transfer flakes of 2D materials from the tape used to mechanically exfoliate to a grid, with some modifications. It was shown that the usage of hotplate in the process of removing the tape from the silicon wafer is important in order to secure larger sample size, however it was also shown that the size and thickness are parameters which are hard to control. The process is shown to be the most sensitive when transferring the sample from the PMMA film to the copper grid, which was due to adhesion of the sample to the PMMA film and the process of dissolving the PMMA film, and even successfully transferred flakes have a possibility of breaking before finally settling onto the grid. The turbulence introduced into the solvent was believed to be the cause of many flakes not sticking to the grid as well as the cause of breaking, and while this turbulence was minimised by the use of the constructed sieve, it was not eliminated. Breakage and rotation of the flakes also causes the orientation to become random, which could possibly cause the different flake to have signals that interfere with each other during measurements. The thickness of the sample was deemed to be thicker than would be preferable for measurements, but were possibly within range of what could give a signal. However, the adhesion of the sample flakes, when successfully transferred, were shown to be good. If breakage could be further minimised, the probability of getting good sized samples onto a grid for further experiments is deemed to be high. As the measured thickness showed that there is margin allowed for the thickness, this would allow for fewer mechanical exfoliations in the preparation step, which would give samples of larger area. As such, the optimal flake should be suspended over as large an area without supporting grid as possible, the orientation should be known for any measurements performed on the sample and there should be no flake of a different orientation close by that could interfere with any measurements.

6 Outlook

2D materials have an interesting future within the electronics industry, as it allows for smaller components, as well as more control over behaviour of the electronics. Graphene already has a large number of applications, and black phosphorus holds several different qualities which could compete with graphene. There are as of now draw backs which holds black phosphorus from more widespread use.

First, the degradation process of black phosphorus means that currently, any applications would need to be completely shielded from ambient air. If the attempts to passivize black phosphorus proves successful, this would mean that black phosphorus samples can be more easily prepared, and will not be sensitive to transportation and light, which is the current case.

Secondly, the health effects of black phosphorus must be understood. Phosphorus is naturally occurring in the human body, and while there are some promise of black phosphorus being possible of use in a biomedical context, the effects of inhalation of the allotrope black phosphorus has as of yet not been examined.

Lastly, there are some parameters of black phosphorus that are not yet looked into, such as heat dissipation. With thin samples of black phosphorus suspended onto a grid, it is possible to perform this type of experiment using electron diffraction, and this would be a natural next step in this process. This type of experiment will be continued by the Ultrafast X-ray Science group at the division for Atomic Physics at the Faculty of Engineering, Lund University. In figure 67, a diffraction pattern of graphite can be seen, with electrons of incident energy 58 keV.

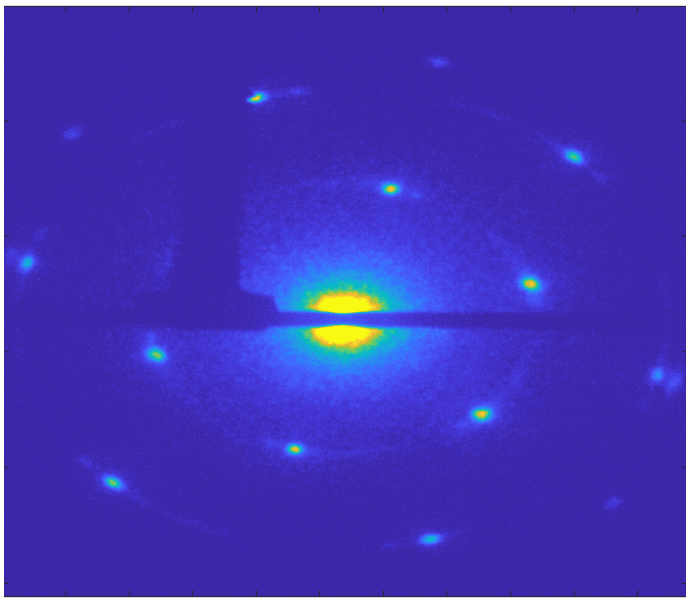

Figure 67: Diffraction pattern of graphite for electrons of incident energy 58 keV.

The centre beam comes from the electrons that do not have any interactions with the material in question, and due to the low scattering cross section, this centre beam have a very high intensity compared to the diffracted spots. This is the reason for the beam block seen in the figure. By using Bragg's law and the angle between the centre beam and the closest circle of rings, which represents the first order of diffraction, the d spacing can be calculated. Conversely, if the d spacing is known, the expected distance of the rings from the centre can be calculated. This can be seen in figure 68.

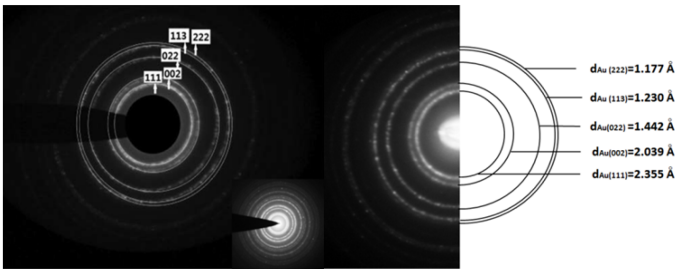

Figure 68: Examples of distance from the centre of different distances between planes of a unit cell d. Image reproduced from reference. [18]

For graphite, if the distance between planes are 2.461 Å, this gives a Bragg angle of 1.19 degrees. For the values of 2.6 Å and 2.16 for two planes in the unit cell of BP according to Y. Lee et. al. [40], this gives the respective Bragg angles 1.12 and 1.35. This means that the diffraction rings of BP can be expected to be close the rings of graphite. Therefore, the diffraction pattern should be possible to see with the set up currently in use.

References

[1] K. S. Novoselov, A. K. Geim, S. V. Morozov, D. Jiang, Y. Zhang, S. V. Dubonos, I. V. Grigorieva, and A. A. Firsov. Electric field effect in atomically thin carbon films. *Science*, 306 (5696):666-669, 2004. ISSN 00368075. doi: 10.1126/science.1102896. URL `https://science.sciencemag.org/content/306/5696/666`.

[2] Pere Miró, Martha Audiffred, and Thomas Heine. An atlas of two-dimensional materials. *Chem. Soc. Rev.*, 43:6537-6554, 2014. doi: 10.1039/C4CS00102H. URL `http://dx.doi.org/10.1039/C4CS00102H`.

[3] Xiaolong Liu, Joshua D. Wood, Kan-Sheng Chen, EunKyung Cho, and Mark C. Hersam. In situ thermal decomposition of exfoliated two-dimensional blackphosphorus. *Journal of Physical Chemistry Letters*, 6, 2015. doi: 10.1021/acs.jpclett.5b00043.

[4] Min Yi and Zhigang Shen. A review on mechanical exfoliation for the scalable production of graphene. *The Royal Society of Chemistry*, 3, 2015. doi: 10.1039/c5ta00252d.

[5] Hanns-Peter Boehm, Ralph Setton, and Eberhard Stumpp. Nomenclature and terminology of graphite intercalculation compounds. *International Union of Pure and Applied Chemistry*, 66(9), 1994. doi: 10.1016/0379-6779(85)90068-2.

[6] Ayman I. Hawari, Ilyad I. Al-Qasir, and Abderrafi M. Ougouang. Investigation of the impact of simple carbon interstitial formations on thermal neutron scattering in graphite. *Nuclear Science and Engineering*, 155(3):449-462, 2007. doi: 10.13182/NSE07-A2676.

[7] Rui Gusmão, Zdenek Sofer, and Martin Pumera. Black phosphorus rediscovered: From bulk material to monolayers. *Angewandte Chemie International Edition*, 56(28):8052-8072, 2017. doi: 10.1002/anie.201610512. URL `https://onlinelibrary.wiley.com/doi/abs/10.1002/anie.201610512`.

[8] Samira Bagheri, Negar Mansouri, and Ermia Aghaie. Phosphorene: A new competitor for graphene. *International Journal of Hydrogen Energy*, 41(7):4085-4095, 2016. ISSN 03603199. doi: https://doi.org/10.1016/j.ijhydene.2016.01.034. URL `http://www.sciencedirect.com/science/article/pii/S0360319915317742`.

[9] Xi Ling, Han Wang, Shengxi Huang, Fengnian Xia, and Mildred S. Dresselhaus. The renaissance of black phosphorus. *Proceedings of the National Academy of Sciences*, 112(15): 4523-4530, 2015. ISSN 00278424. doi: 10.1073/pnas.1416581112. URL `https://www.pnas.org/content/112/15/4523`.

[10] Andrey Chaves, Wei Ji, Jesse Maassen, Traian Dumitrică, and Tony Low. Theoretical overview of black phosphorus. *2D Materials*, page 381–412, 2017. doi: 10.1017/9781316681619.022. URL `http://dx.doi.org/10.1017/9781316681619.022`.

[11] Andres Castellanos-Gomez, Leonardo Vicarelli, Elsa Prada, Joshua O Island, K L Narasimha-Acharya, Sofya I Blanter, Dirk J Groenendijk, Michele Buscema, Gary A Steele, J V Alvarez, Henny W Zandbergen, J J Palacios, and Herre S J van der Zant. Isolation and characterization of few-layer black phosphorus. *2D Materials*, 1(2):025001, jun 2014. doi: 10.1088/2053-1583/1/2/025001. URL `https://doi.org/10.1088%2F2053-1583%2F1%2F2%2F025001`.

[12] Haiwei Du, Xi Lin, Zhemi Xu, and Dewei Chu. Recent development in black phosphorus transistors. *J. Mater. Chem. C*, 3, 07 2015. doi: 10.1039/C5TC01484K.

[13] Joshua D. Wood, Spencer A. Wells, Deep Jariwala, Kan.Sheng Chen, EunKyung Cho, Vinod K. Sangwan, Xiaolong Liu, Lincoln J. Lauhon, Tobin J. Marks, and Mark C. Hersam. Effective passivation of exfoliated black phosphorus transistorsagainst ambient degradation. *Nano Letters*, 14, 2014. doi: 10.1021/nl5032293.

[14] Changbae Hyun, Jong Hun Kim, Jong-Young Lee, Gwan-Hyoung Lee, and Kwang S. Kim. Atomic scale study of black phosphorus degradation. *Royal Society of Chemistry*, 10, 2020. doi: 10.1039/c9ra08029e.

[15] Likai Li, Yijun Yu, Guo Jun Ye, Qingqin Ge, Xuedong Ou, Hua Wu, Donglai Feng, Xian Hui CHen, and Yuanbo Zhang. Black phosphorus field-effect transistors. *Nature Nanotechnology*, 9:372-377, may 2014. doi: 10.1038/nnano.2014.35. URL `https://doi.org/10.1038/nnano.2014.35`.

[16] Jane Ru Choi, Kar Wey Yong, Jean Yu Choi, Azadeh Nilghaz, Yang Lin, Jie Xu, and Xiaonan Lu. Black phosphorus and its biomedical applications. *Theranostics*, 8(4), 2018. doi: 10.7150/thno.22573.

[17] K Kanaya and S Okayama. Penetration and energy-loss theory of electrons in solid targets. *Journal of Physics D: Applied Physics*, 5(1):43-58, jan 1972. doi: 10.1088/0022-3727/5/1/308. URL `https://doi.org/10.1088%2F0022-3727%2F5%2F1%2F308`.

[18] Mohsen Asadi Asadabad and Mohammad Jafari Eskandari. Electron diffraction. *Modern Electron Microscopy in Physical and Life Sciences*, 2016. doi: 10.5772/61781.

[19] S. Tanuma, C. J. Powell, and D. R. Penn. Calculations of electron inelastic mean free paths. ix. data for 41 elemental solids over the 50 ev to 30 kev range. *Surface and Interface Analysis*, 43(3):689-713, 2011. doi: 10.1002/sia.3522. URL `https://onlinelibrary.wiley.com/doi/abs/10.1002/sia.3522`.

[20] Henrique B. Ribeiro, Marcos A. Pimenta, Christiano J. S. de Matos, Roberto Luiz Moreira, Aleksandr S. Rodin, Juan D. Zapata, Eunezio A. T. ds Souza, and Antonio H. Castro Neto. Unusual angular dependence of the raman response in black phosphorus. *American Chemical Society*, 7, 2015. doi: 10.1021/acsnano.5b00698.

[21] Henrique B. Ribeiro, Marcos A. Pimenta, and Christiano J. S. de Matos. Raman spectroscopy in black phosphorus. *Journal of Raman Spectroscopy*, 49, 2018. doi: 10.1002/jrs.5238.

[22] Xi Ling, Shengxi Huang, Eddwi H. Hasdeo, Liangbo Liang, William M. Parkin, Yuki Tatsumi, Ahmad R. T. Nugraha, Alexander A. Puretzky, Paul Masih Das, Bobby G. Sumpter, David B. Geohegan, Jing Kong, Riichiro Saito, Marija Drndic, Vincent Meunier, , and Mildred S. Dresselhaus. Anisotropic electron-photon and electron-phonon interactions in black phosphorus. *Nano Letters*, March 2016. doi: 10.1021/acs.nanolett.5b04540.

[23] Jungcheol Kim, Jae-Ung Lee andJinhwan Lee, Hyo Ju Park, Zonghoon Lee, Changgu Lee, and Hyeonsik Cheong. Anomalous polarization dependence of raman scattering and crystallographic orientation of black phosphorus. *Nanoscale*, 7, 2015. doi: 10.1039/c5nr04349b.

[24] Juanxia Wu, Nannan Mao, Liming Xie, Hua Xu, and Jin Zhang. Identifying the crystalline orientation of black phosphorus using angle-resolved polarized raman spectroscopy. *Angewandte Chemie International Edition*, 54, 2015. doi: 10.1002/anie.201410108.

[25] Hugo Gonçalves, Joel Fernandes, Cacilda Moura, Peter Schellenberg, Michael Belsley, and Luís Alves. Easy process to obtain suspended graphene flakes on TEM grids. *Materials Research Express*, 2(5):055602, apr 2015. doi: 10.1088/2053-1591/2/5/055602. URL `https://doi.org/10.1088%2F2053-1591%2F2%2F5%2F055602`.

[26] Sigma-Aldrich Sweden AB. *Material safety data sheet: Black phosphorus.* Sigma Aldrich Sweden AB, Stockholm, Sweden, 2020.

[27] Sigma-Aldrich Sweden AB. *Material safety data sheet: Acetone.* Sigma Aldrich Sweden AB, Stockholm, Sweden, 2019.

[28] Sigma-Aldrich Sweden AB. *Material safety data sheet: Isopropanol.* Sigma Aldrich Sweden AB, Stockholm, Sweden, 2020.

[29] Hyejin Jang, Joshua D. Wood, Cristopher R. Ryder, Mark C. Hersam, and David G. Cahill. Anisotropic thermal conductivity of exfoliated black phosphorus. *Advanced Matter*, 27, 2015. doi: 10.1002/adma.201503466.

[30] Josh P. Thompson, M. Hasan Doha, Peter Murphy, Jin Hu, and Hugh O.H. Churchill. Exfoliation and analysis of large-area, air-sensitive two-dimensional materials. *Journal of Visualised Experiments*, 143, 2019. doi: 10.3791/58693.

[31] Sigma-Aldrich Sweden AB. *Material safety data sheet: Poly(methyl methacrylate).* Sigma Aldrich Sweden AB, Stockholm, Sweden, 2020.

[32] Ted Pella Microscopy Products for Science and Industry. *Gilder TEM Grids for Transmission Electron Microscopy.* Ted Pella Microscopy Products for Science and Industry, viewed March 13 2020. URL `https://www.tedpella.com/grids_html/gilder.htm`.

[33] Hildegard H. Crowley, Department of Biological Sciences, University of Denver, and Denver CO. 80208. *Grids: Shiny Side vs Dull Side?* Electron Microscopy Sciences, viewed August 30 2020. URL `https://www.emsdiasum.com/microscopy/technical/techtips/shiny_side.aspx`.

[34] Sigma-Aldrich Sweden AB. *Material safety data sheet: Toluene.* Sigma Aldrich Sweden AB, Stockholm, Sweden, 2020.

[35] I Yu Evchuk, RI Musii, RG Makitra, and RE Pristanskii. Solubility of polymethyl methacrylate in organic solvents. *Russian Journal of Applied Chemistry*, 78(10):1576-1580, June 2005. doi: 1070-4272/05/7810-1576.

[36] Recep Zan, Chris Muryn, Ursel Bangert, Philip Mattocks, Paul Wincott, David Vaughan, Xuesong Li, Luigi Colombo, Rodney S. Ruoff, Bruce Hamilton, and Konstantin S. Novoselov. Scanning tunnelling microscopy of suspended graphene. *Nanoscale*, 4:3065-3068, 2012. doi: 10.1039/C2NR30162H. URL `http://dx.doi.org/10.1039/C2NR30162H`.

[37] 2D Semiconductors. *Monolayer Black Phosphorus Solution.* 2D Semiconductors, viewed 9 March 2020. URL `https://www.2dsemiconductors.com/monolayer-black-phosphorus-solution/`.

[38] B.E.A Saleh and M.C. Teich. *Fundamentals of Photonics.* John Wiley and Sons, Inc., 2007.

[39] Nannan Mao, Jingyi Tang, Liming Xie, Juanxia Wu, Bowen Han, Jingjing Lin, Shibin Deng, Wei Ji, Hua Xu, Kaihui Liu, Lianming Tong, and Jin Zhang. Optical anisotropy of black phosphorus in the visible regime. *American Chemical Society*, 138, 2016. doi: 10.1021/jacs.5b10685J.

[40] Y. Lee, J-Y Yoon, D. Scullion, J. Jang, E. J. G. Santos, HY Jeong, and K. Kim. Atomic-scale imaging of few-layer black phosphorus and its reconstructed edge. *Journal of Physics D: Applied Physics*, 2017. doi: 10.1088/1361-6463/aa5583.

Appendix A

Calculations: Sample thickness

To calculate the thickness of the sample, the following method was used. As presented in the method, a laser of 532 nm is directed onto a silicon wafer. The intensity of the Raman peak of the 521 cm^{-1} vibrational mode of silicon is measured by a spectrometer. This intensity is the reference value. The laser is then directed onto the BP sample placed on the silicon wafer. The decrease of the intensity of the Raman peak of silicon is then assumed to be caused by absorption in the BP sample, as well as reflections due to refraction between the different materials. For the incident laser wavelength used for the measurement, 532 nm, the corresponding energy is $E = \frac{hc}{\lambda} = 2.33$ eV. From figure 2 presented by Ling et. al. in the article *Anisotropic Electron-Photon and Electron-Phonon Interactions in Black Phosphorus* [22], the values of absorbance A are read as $A_{AC} = 1.11$ for the AC direction and $A_{ZZ} = 0.65$. The values of absorbance are used to calculate the transmission as follows

$$\begin{aligned} A = \log_{10}(T) \Rightarrow \\ T_{AC} = 10^{-A_{AC}} = 0.0776 \\ T_{ZZ} = 10^{-A_{ZZ}} = 0.224 \end{aligned} \tag{7}$$

The ratio $\frac{I}{I_0}$ is replaced by the transmission T in the Beer-Lambert equation 6, and with the still assumed value of the thickness as 225 nm, the absorption coefficient α is calculated

$$\begin{aligned} I = I_0 \exp(-\alpha z) \Rightarrow \alpha = \frac{\log_{10}(T)}{-225 \cdot 10^{-9}} \Rightarrow \\ \alpha_{AC} = \frac{\log_{10}(T_{AC})}{-225 \cdot 10^{-9}} = 1.14 \cdot 10^7 \text{ m}^{-1} \\ \alpha_{ZZ} = \frac{\log_{10}(T_{ZZ})}{-225 \cdot 10^{-9}} = 6.65 \cdot 10^6 \text{ m}^{-1} \end{aligned} \tag{8}$$

By reinserting the calculated value for the absorption coefficient into the Beer-Lambert equation with the measured ratio between the counts for Si with and without BP presented in table 5 as the ratio $\frac{I}{I_0}$, an approximate value for the thickness z can be calculated. Before calculating the thickness, the losses due to reflection from the sample has to be considered. The simple model used, presented in figure 69, assumes that there is loss of intensity from the transitions between air and sample.

The ratio of reflected light is given by $r = \frac{n_x - n_y}{n_x + n_y}$ for a beam of light passing from a material of refractive index n_x to a material of n_y. [38] The refractive index is

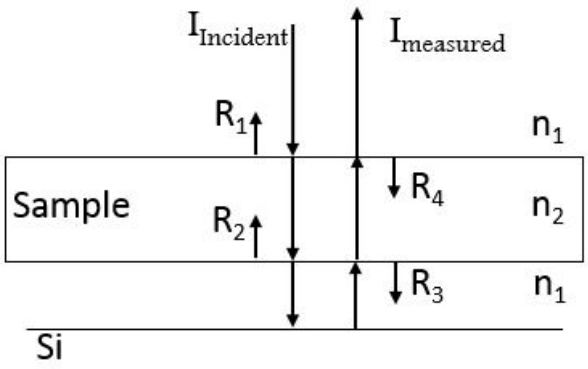

Figure 69: The incoming light intensity $I_{incident}$, the measured intensity $I_{measured}$ the loss of intensity from reflections between air and sample (BP) R_1 and R_3, the loss from reflections between sample and air R_2 and R_4 and the refractive index n_1 for air and n_2 for BP.

$n_1 = 1$ for air, 2.6 for the AC direction and 3.1 for the ZZ direction of BP, as n_2. The values of the refraction index of BP are taken from figure 5 of the supporting material presented by Mao et. al. in the article *Optical Anisotropy of Black Phosphorus in the Visible Regime* [39]. The intensity of the reflected light is $R = r^2$ and the fraction of the transmitted intensity T is then given by $T = 1 - R$. [38] This then gives the intensity loss of the signal due to refracting as follows

$$\begin{aligned} I_{incident} &= T_{fraction of transmitted intensity} I_{measured} \Rightarrow \\ I_{incident} &= (1-R_1)(1-R_2)(1-R_3)(1-R_4) I_{measured} \\ &= (1-(\frac{n_1-n_2}{n_1+n_2})^2)^2 (1-(\frac{n_2-n_1}{n_2+n_1})^2)^2 I_{measured} \Rightarrow \\ &\text{Transmitted intensity of the AC direction: } 41\% \\ &\text{Transmitted intensity of the ZZ direction: } 30\% \end{aligned} \tag{9}$$

The absorption coefficient α, together with the ratio between the highest and lowest intensity presented in table 5, corrected for the signal loss, is reinserted into the Beer-Lambert equation. Then finally the result is divided by 2, to account for the laser beam passing through the sample twice, resulting in twice the amount of signal loss. An approximate value of z is then given as follows

$$\begin{aligned} I = I_0 \exp(-\alpha \frac{1}{z}) \Rightarrow z = \frac{1}{-\alpha} \log(\frac{I}{I_0} \cdot \frac{1}{\text{Transmitted intensity}}) \Rightarrow \\ z_{AC} = \frac{1}{-2\alpha_{AC}} \log(0.2136 \cdot \frac{1}{0.41}) = 30 \text{ nm} \\ z_{ZZ} = \frac{1}{-2\alpha_{ZZ}} \log(0.1900 \cdot \frac{1}{0.30}) = 33 \text{ nm} \end{aligned} \tag{10}$$